4D Printing of Shape Memory Polymers, Blends, and Composites and Their Advanced Applications: A Comprehensive Literature Review

Mohamed Ali Kouka, Fethi Abbassi, Mohamed Habibi, France Chabert, Ali Zghal, Christian Garnier

Four-dimension printing of shape memory polymers, blends and composites and their advanced applications: A comprehensive literature review

Mohamed Ali Kouka [a, b], *Fethi Abbassi* [c]*, *Mohamed Habibi* [d*], *France Chabert* [b], *Ali Zghal* [a] *and Christian Garnier* [b*]

[a] *LMPE, ENSIT, University of Tunis, 5 Avenue Hussein, BP, 56, Bâb Manara, 1008, Tunisia*
[b] *Laboratoire Génie de Production (LGP), University of Toulouse, INP-ENIT, 47 Av. d'Azereix, 65016 Tarbes, France,*
[c] *College of Engineering and Technology, American University of the Middle East, Kuwait.*
[d] *Department of mechanical engineering, Université du Québec à Trois-Rivières, Quebec, Canada.*

**Corresponding authors: Fethi Abbassi fethi.abbassi@aum.edu.kw,*
Mohamed Habibi mohamed.habibi@uqtr.ca,
Christian Garnier christian.garnier@enit.fr

Keywords: 3D printing, 4D printing, Composites, Shape memory polymers, Smart materials

Abstract

4D printing is defined as the additive manufacturing process of smart (stimuli-responsive) materials. Shape memory materials are sensitive to specific stimuli such as heat, electricity, magnetic fields, etc., which can change their form or properties. This characteristic gives the material a dynamic behavior over time (the 4th dimension). The application of the 4D printing technique is currently being explored in various fields, including soft robotics, electrical devices, deployable structures, medical implants, and medicine delivery systems. This paper first examines the fundamentals of 3D printing techniques, their advantages and limitations. Then, the shape memory materials are categorized and reviewed according to their type (shape memory polymers, shape memory composites, polymer blends, etc.) and stimulus responsiveness. Lastly, different properties of shape memory materials like shape memory effect, thermo-mechanical properties, and their compatibility with different types of additive manufacturing processes, are discussed.

Abbreviations:

3DP: Three-dimensional printing

ABS: Acrylonitrile butadiene styrene

AESO: Acrylated epoxidized soybean oil

Ag@CNF: Silvercoated carbon nanofiber

AM: Additive manufacturing

AT: Aniline trimer

AT-PEI: Aniline tetramer-grafted-polyethylenimine

AUD: Aliphatic urethane diacrylate

BFDGE: Bisphenol F diglycidyl ether

BA: n-butyl acrylate

BAPO: Phenylbis (2,4,6-trimethyl benzoyl) phosphine oxide

BIS: Beam interference solidification

BMA: Benzyl methacrylate

BP: Benzophenone

BPA: Bisphenol A ethoxylate dimethacrylate

BPM: Ballistic particle manufacturing

CB: Carbon black

CMC: Carboxymethyl cellulose

CNC: Cellulose nanocrystals

CNF: Carbon nanofiber

CNT: Carbon Nano Tube

DCM: Dichloromethane

DEGDMA: Di(ethylene glycol) dimethacrylate

DEGDA: Di(ethyleneglycol) diacrylate

DGEDA: Bisphenol A diglycidyl ether diacrylate

DGEBA: Diglycidyl ether of bisphenol A

DIW: Direct ink writing

DLP: Digital Light Processing

DMD: Direct metal deposition

DMLS: Direct metal laser sintering

EA: Epoxy acrylate

Eb: Ebecryl 8232

EBM: Electron beam manufacturing

EDDET: 2,2'-(ethylenedioxy) diethanethiol

EHA: 2-ethylhexyl acrylate

ESBO: Epoxidized soybean oil

F127DA: F127 diacrylate

FDM: Fused deposition modelling

FFF: Fused filament fabrication

GA: Glutaraldehyde

g-GO: Graphene oxide

HBC-MA: Hydroxybutyl methacrylated chitosan

HDDA: 1, 6-hexanediol diacrylate

HEA: 2-Hydroxyethyl acrylate

HEMA: 2-hydroxyethyl methacrylate

HIS: Holographic interference solidification

HS: Hard segments

IBOA: Isobornyl acrylate

IJP: Inkjet printing

LDPE: Low density polyethylene

LENS: Laser engineered net shaping

LOM: Laminated object manufacturing

LPD: Laser powder deposition

LTP: Liquid thermal polymerization

MJM: Multi-jet modelling

MS: Mercaptosiloxane

MTHPA: Methyl tetrahydrophthalic anhydride

MWCNT: Multi-walled carbon nanotube

NdFeB: Neodymium-iron-boron

P2VP: Poly(2-vinylpyridine)

PBS: Phosphate-buffered saline

PC: Poly(Bisphenol A carbonate)

PCL: Polycaprolactone

PDMS: Polydimethylsiloxane

PE: Polyethylene

PEBA: Polyether block amide

PEEK: Poly (ether ether ketone)

PEGDA: Poly(ethylene glycol) diacrylate

PEGDMA: Methacrylate poly (ethylene glycol) dimethacrylate

PEO: Polyethylene oxide

PET: Poly(ethylene terephthalate)

PEW: Polyethylene wax

PI184: 1-hydroxycyclohexyl phenyl ketone

PLA: Polylactic-acid

PMA: Polymethylacrylate

PMMA: Poly methacrylate

PNIPAAm: Poly(N-isopropylacrylamide)

PP: Polypropylene

PPG: Polypropyleneglycol

PTFE: Polytetrafluoroethylene

PTMO: Poly(tetrahydrofuran)

PU: Polyurethane

PUA: Polyurethane acrylate

PVA: poly (vinyl alcohol)

PVDF: Polyvinylidene fluoride

RM82: 1,4-bis-[4-(6-acryloyloxhexyloxy) benzoyloxy]-2-methylbenzene

SEBS: Styrene-b-(ethylene-cobutylene)-b-styrene

SEM: Scanning Electron Microscope

SFP: Solid foil polymerization

SGC: Solid ground curing

SLA: Stereolithography

SLC: Selective laser cladding

PLMC: D,L-lactide-co-trimethylene carbonate

SLM: Selective laser melting

SLS: Selective laser sintering

SMA: Shape memory alloy

SMC: Shape memory composite

SMM: Shape memory material

SMP: Shape memory polymer

SPIO NP: Iron oxide nanoparticle

SPS: Sodium persulfate

SS: Soft segments

TAIC: Triallyisocyanurate

tBA: *Tert*-butyl acrylate

T_g: Glass transition temperature

T_m: Melting temperature

TMPTA: Trimethylolpropane triacrylate

TMPTA: Trimethylolpropane ethoxylate triacrylate

TPI: Trans-1, 4-polyisoprene

TPU: Thermoplastic polyurethane

UPy: 2-ureido-4[1H]-pyrimidinone

VS: Vinylsiloxane

1. Introduction

Additive manufacturing (AM), commonly known as three-dimensional (3D) printing, is a manufacturing technique based on the layer-by-layer principle to produce 3D physical objects [1]. It can be traced back as early as the 1980s [2]. Since then, AM has seen advancements in printing techniques and materials' versatility. Nowadays, this technology has become very accessible thanks to the affordable cost of 3D printers.

Unlike conventional manufacturing processes such as casting, machining, or forming, 3D printed objects are made by deposition of successive thin layers of material [3]. This technique allows the production of unique, custom-made, and complex structures [4] from a vast choice of materials [5]: metals [6], alloys [7], polymers [8], ceramics [9], concrete [10] or composites [11].

AM techniques are typically in the form of: material extrusion, in which material is extruded through a nozzle; material jetting, in which material droplets are selectively deposited; and vat photopolymerization, in which liquid photopolymer in a vat is selectively cured by light-activated polymerization [12]. As shown in **Table 1,** AM processes can be classified based on the technology or the material used. The raw material can be either in a powder-state, liquid-state or solid-state.

AM is mainly used for manufacturing custom parts, including prototypes and small series products. Nevertheless, the industry of 3D printing has seen increasing growth. It is adopted in robotics [13], biomedicine [14], and aeronautics [15], and self-actuating devices [16]. 3D printing has garnered substantial interest not only from academics but also from the industry due to its potential in the smart manufacturing establishment.

Table 1. 3D printing processes depending on the technology and materials

Material state	Technology	Process
Powder	Laser Melting	SLS – SLM – DMLS – DMD – LENS – SLC – LPD
	Material Jetting	3DP
	Electron Beam	EBM
Liquid	Laser Polymerization	SLA – SGC – LTP – BIS – HIS
	Material Jetting	3DP – IJP – MJM – BPM – Thermojet
Solid	Thermal Extrusion	FDM – FFF – Robocasting
	Material Adhesion	LOM – SFP

The introduction of shape-memory materials in 3D printing has given rise to a fourth dimension, also known as 4D printing. 4D printing can be defined as the process by which a 3D printed object can modify its structure and change shape under the influence of an external energy source [17], such as temperature [18], light [19] or other environmental stimuli [20]. Skylar Tibbits first introduced the concept of 4D printing in 2013 in a TED conference. The major advance of 4D printing is the ability of materials to change shape over time [21].

A 4D printed object is obtained in the same way as a 3D printed object. The difference is that 4D technology uses advanced programmable materials that add new functionality to the object over time, for example to change their shape [22], to self-assemble [23], or to self-heal [24]. Their dynamic properties allow these smart materials to be (potentially) applicable in a wide range of fields, such as soft robotics [25], aerospace [26], and biomedical implants [27]. **Figure 1** summarizes the origins of 3D and 4D printing and how they have progressed.

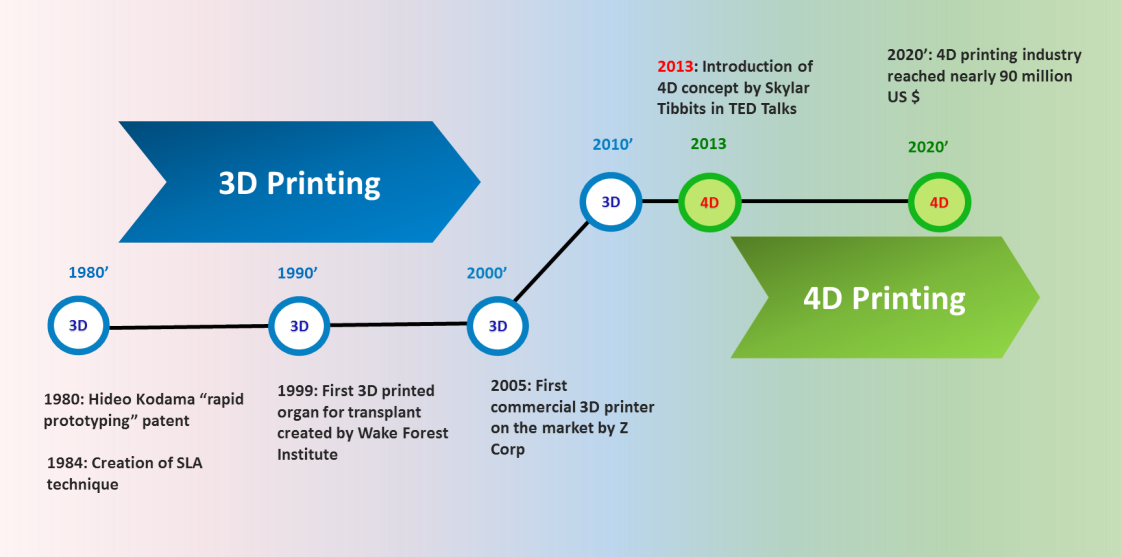

Figure 1. Evolution of additive manufacturing techniques with key history dates.

The printing agent is a shape memory material (SMM). To obtain precise and predictable transformations from a material, it is necessary to structure it in a particular way and then activate it with a stimulus. The type of the required stimulus varies depending on the intrinsic properties of the material chosen [28]. It can be temperature, humidity, pressure, vibrations, or electricity. Shape memory materials can be classified according to their base material: a shape memory polymer (SMP) [29, 30], a shape memory alloy (SMA) [31] or a shape memory composite (SMC) [32].

As an emerging new technology, 4D printing is an alluring field of research. The number of scientific papers published each year is growing exponentially. For instance, from 2017 to 2021, the number of papers published in sciencedirect.com increased from 167 to 621 as attested in **Figure 2.a**. They cover different aspects, such as the printing techniques, the development of

the SMMs, and their applications. Moreover, these scientific publications related to 3D and 4D printing are reported in fields such as material science [33], mechanical engineering [34], chemistry [35], and computer science [17] as shown in **Figure 2.b**.

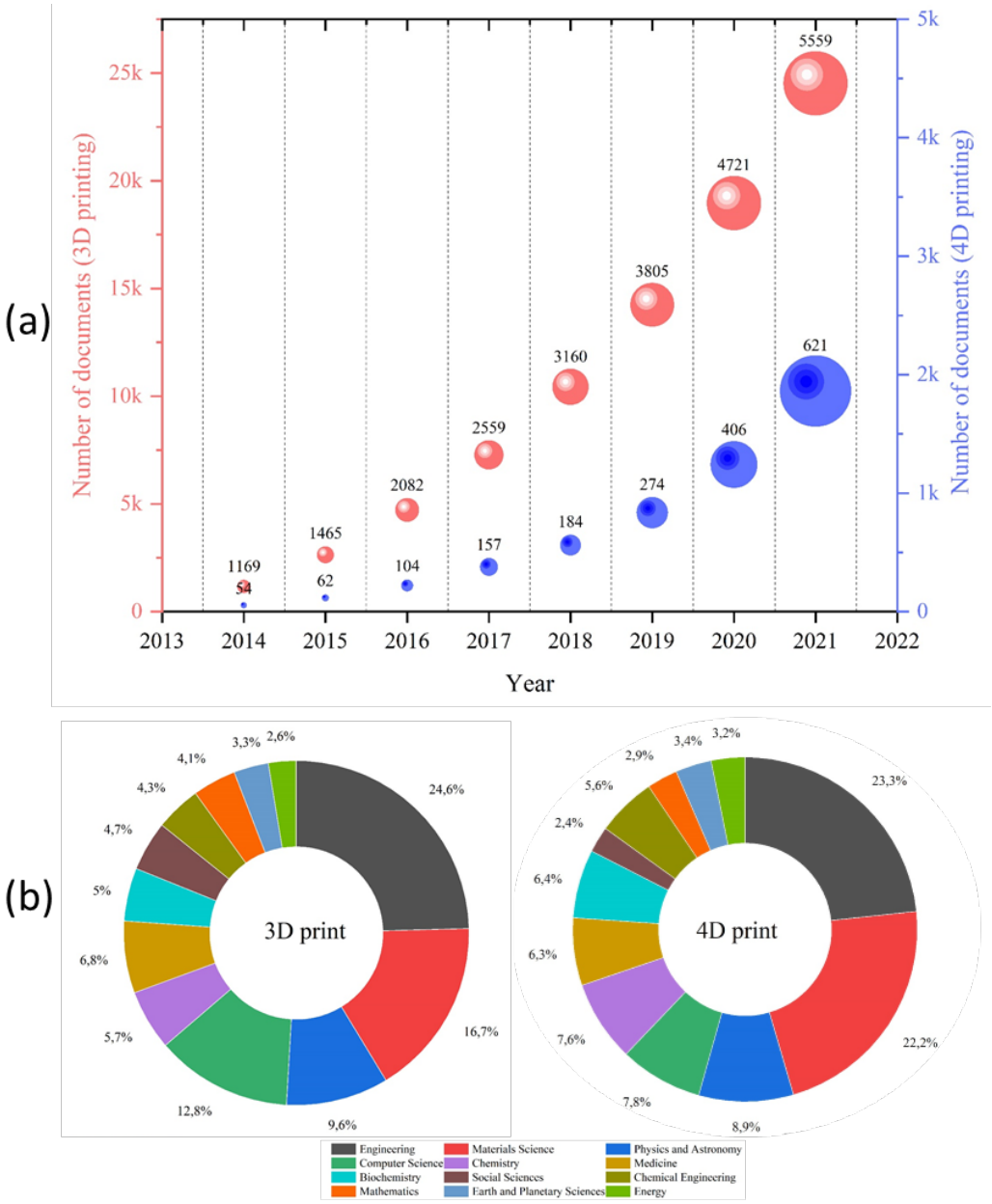

Figure 2. (a) Evolution of the numbers of scientific publications about 3D and 4D printing in sciencedirect.com (b) Research fields publications of 3D printing and 4D Printing (Source: scopus.com).

4D printing is a flourishing industry even though it has yet to be widely adopted in large-scale manufacturing. It is expected to continue to grow as it has already been used in various industrial applications such as electronics [36], automobiles [37], and textiles [38].

2. Shape memory effect

Polymers are generally classified into two classes. The first one is thermosets. Their structure consists of a tridimensional network of molecules. Their morphology is amorphous, meaning without ordered molecule organization. They are formed from oligomers bonded together by covalent cross-linking upon heating or UV radiation**.** The second class gathers thermoplastics, which comprise linear and branched macromolecules linked together by weak bonds (Hydrogen and/or van der Waals bonds). Upon heating, the weak bonds are broken, the macromolecules are free to slide over each other, resulting in material flowing. Thanks to the reversibility of weak bonds, thermoplastics are endowed with astounding properties: they are malleable enough to be shaped into complex geometry in their melted state, and they turn to solid behavior on cooling.

Thermoplastics can give either amorphous or semi-crystalline structures. Their ability to crystallize depends on the regularity of monomer sequence, the flexibility of polymer backbone, macromolecular weight, amount of weak bonds, presence of fillers and plasticizers. SMPs are obtained from both thermoplastic and thermoset polymers.

In the case of semi-crystalline shape memory polymers, the transition temperature at which the shape memory effect is triggered, is the melting temperature. At this temperature, the mobility of the chain is activated by the transition from a crystalline to a completely amorphous phase, thus, playing the role of an exchange domain. These systems are generally block copolymers composed of immiscible blocks [39]. Block copolymers are macromolecules comprising a linear arrangement of two or more chemically different chain portions joined by covalent bonds. The polymer chains are covalently tethered, preventing a macroscopic separation. The structural organization takes place at the molecular scale (5–100 nm), producing complex nanostructures with various morphologies [40].

This enables nanophase segregation, which leads to rigid and flexible domains. Both domains keep the temporary and permanent forms stable, and ensure there is an exchange area between

them [41]. During the programming step, the polymer is heated above the melting temperature of the crystallites. This leads to a completely amorphous state, which increases the mobility of the chain segments during the deformation of the material into its temporary form. The cooling under stress leads to the recrystallization of the crystalline domains, allowing the fixation of a new stable shape over time. During the recovery step, the material is heated without stress above the melting temperature of the crystallites. Due to the rigid block's physical cross-linking nodes stopping the chains from moving, the shape of the block stays the same [42, 43].

As for semi-crystalline polymers, amorphous systems are also composed of blocks that enable physical cross-linking or domain exchange. When a good segregation between the hard and soft blocks is established, the glass transition temperature (T_g) of the soft block plays the role of a reversible transition in the shape memory phenomenon. In the case of partial miscibility of the two phases, it is an intermediate T_g, between the T_g of the soft block and that of the hard block, which dictates this property. It is above the T_g, by making the chain segments more mobile, that it is then possible to deform and reform the material effectively [17].

3. Additive Manufacturing Processes

There are many AM technologies. Among them, material extrusion focuses primarily on a thermoplastic filament extrusion process. Fused Filament Fabrication (FFF) technology, known as its commercial name Fused Deposit Modeling (FDM), is the most common and accessible in this category. Other technologies use powder fusion and involve the use of a laser. SLM (Selective Laser Melting) and SLS (Selective Laser Sintering) are best known. The photopolymerization in a resin bath uses the scanning of a laser (SLA). 3D printing technologies differ in the materials used, how they are used, and how the layers are created (**Table 2**). Such differences determine the precision of the part, its material properties, and its mechanical properties [3]. The strengths and weaknesses of the main technologies are exposed in this section.

Table 2. Summary of different additive manufacturing techniques

3D Process	FDM	SLA	DLP	DIW	IJP
Feed state	Solid	Liquid	Liquid	Liquid	Powder
Materials	Thermoplastics: PC, ABS, PLA, etc.	Photocurable resin (epoxy or acrylate resins)	Metamaterials and elastomers	Ceramics, viscoelastic materials	Photopolymers, bio-inks
Functioning principal	Extrusion and layer-by-layer deposition	Laser scanning and UV curing	Liquid solidification and layer-by-layer deposition	Viscoelastic inks solidification and layer-by-layer deposition	Powder sintering and layer-by-layer solidification
Resolution [µm]	50-200	10	15-100	100-600	20-200
Advantages	Low cost, good resistance, multi-material capacity	High resolution and precision	high printing speed	Multi-material printing	Good resolution, multi-material printing, low cost, biocompatibility
Limitations	Anisotropy, nozzle clogging	Materials limitation, cytotoxicity, high cost	Materials limitation, high maintenance cost	Materials limitation, high maintenance cost, low printing speed	Materials limitation, low printing speed,
References	[44, 45]	[46, 47]	[48, 49]	[50, 51]	[52, 53]

3.1. Fused Filament Fabrication

The fused filament fabrication (FFF) process, or plastic jet printing, was developed in the late 1980s [44]. In contrast to other additive manufacturing processes, extrusion systems are relatively inexpensive and simple to use [44]. The process starts with the preheating of the extrusion head (around 200°C, depending on the thermal transitions of the material), necessary to allow the material to go from a solid-state to a malleable state (shaping temperature) [54, 55]. Once the machine is heated, a material thread is extruded onto a platform through a nozzle moving on two or three axes, depending on whether the platform is fixed or mobile. The platform goes down with each newly applied layer until the end of the printing of the object [44].

Due to their rapid melting when heated and their ability to recover their mechanical properties after cooling, only thermoplastic polymers are suited for this type of 3D printing technique [56]. Initially limited to a few thermoplastic polymers, this technology is now compatible with a wide range of thermoplastic composite materials, including filaments composed of a mixture of polymer and wood [57], stone, or ceramics. It is also possible to print food products by making adaptations to the extrusion head [58].

Extrusion process parameters significantly influence the material's characteristics and the properties of the printed parts. Barletta et al. [59] printed geometrically complex specimens (**Figure 3.a**) via FFF process using PLA filaments. A correlation between manufacturing parameters and manufactured parts' properties was established. For instance, increasing the nozzle's temperature from 180 °C to 210 °C and the layer thickness from 0.15 mm to 0.30 mm led to increased compressive resistance. Inversely, when the deposition speed increases, the compressive load as well as the recovery rate and times all decrease. Furthermore, the specimens printed with higher layer thickness exhibited more homogeneity and compactness resulting in better shape recovery. When the nozzle temperature is set to 210 °C, the viscosity of PLA filaments is more adapted to the 3D printing process. In contrast, at lower temperature the material is more viscous and the extrusion process is more difficult.

Ginoux et al.[60] studied the impact of 3D printing parameters on the mechanical properties of FFF-printed parts. The material used is a PLA polymer reinforced with layered silicate. The T_g and T_m of the PLA are 60 °C and between 170 °C and 180 °C, respectively. The specimens manufactured at an optimal printing speed equal to 75 $mm.s^{-1}$, showed the least defects and porosity. Specimens printed at lower and higher speed exhibited triangular and elongated voids, respectively. The highest tensile modulus and tensile strength are equal to 1397 MPa and 59.4 MPa, respectively, and both were obtained at 75 $mm.s^{-1}$ printing speed and 215 °C extrusion temperature.

Bakrani Balani [61]et al. studied the impact of the printing parameters on the rheological and mechanical properties of FFF-printed parts using PLA polymer. Then the nozzle diameter was increased from 0.3 mm to 2 mm while maintaining the temperature at the liquefier at 195 °C. It was observed that the material viscosity increased from 295 Pa.s to 1850 Pa.s. When the nozzle diameter was minimal (0.3 mm) the shear rate and the inlet velocity reached their highest: 7800 s^{-1} and 484 $mm \cdot s^{-1}$, respectively. The produced parts lost their surface quality as the nozzle diameter increases. To achieve a stable extrusion process and a good surface precision, the optimal parameters were determined: the nozzle diameter should be equal to 0.4 mm or 0.5 mm while the layer thickness and feed rate must be maintained inferior to 0.4 mm and 30 $mm.s^{-1}$, respectively.

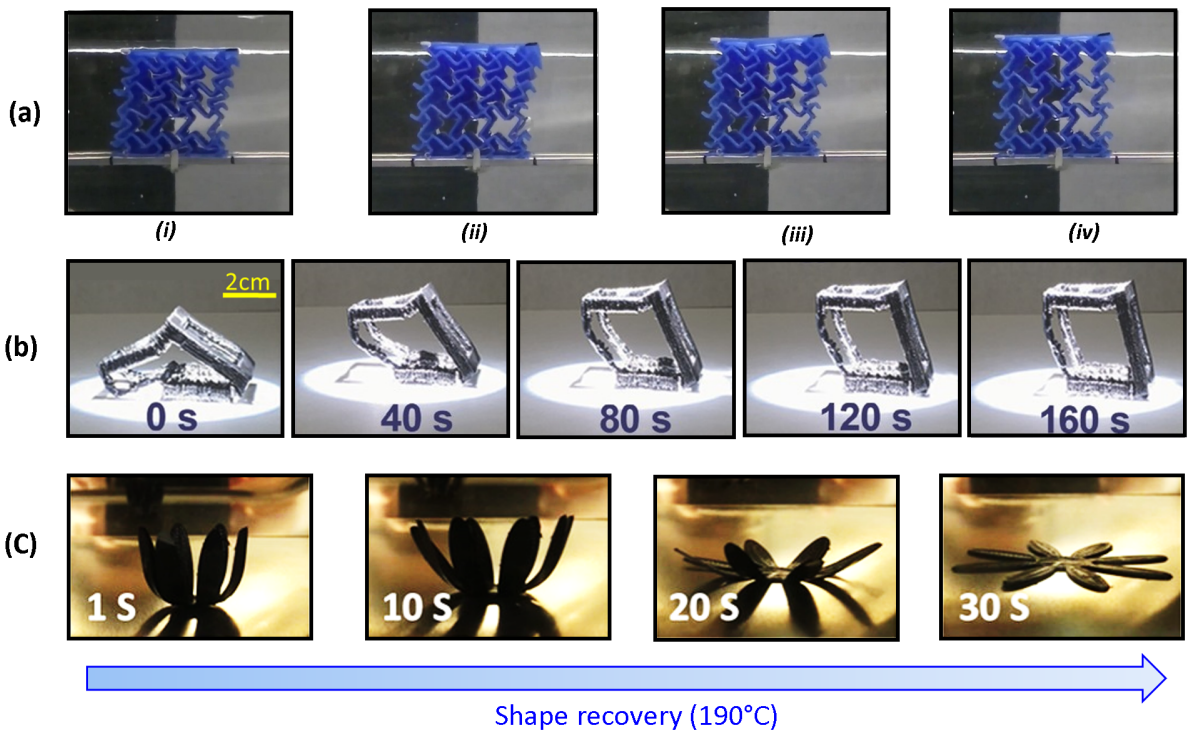

Figure 3. FFF printed parts with shape memory effect: a) Auxetic structure made from PLA. Reproduced with permission. [59] Copyright 2021, Elsevier. b) Light responsive cubic frame. Reproduced with permission. [62] Copyright 2017, Wiley. c) Heat-responsive SMP flower. Reproduced with permission. [63] Copyright 2020, American Chemical Society.

Vanaei et al.[64] used the same material and AM technique to investigate the influence of the process parameters on the mechanical properties of the printed parts. The study showed that the ultimate tensile strength and the elastic modulus decreased both to 56.5 MPa and 1 GPa, respectively, when the print speed increased to 60 $mm.s^{-1}$. Inversely, as the layer thickness increases to 0.3 mm, the ultimate tensile strength and the elastic modulus both increase to 61.5 MPa and 1.3 GPa, respectively. Similar studies focused on other materials such as poly (ether ether ketone) (PEEK) [65] and ABS polymers [66] or other process parameters such as the nozzle geometry [67], deposition orientation [68] and post-printing heat treatment [69].

This category of printing techniques can be easily manipulated and has a wide range of printing materials [44]. Its main disadvantages are the potentially weak adhesion between layers, which affects the strength of the produced parts [70], and the irregular distribution of the heat gradient across the parts, which can lead to the bending of the edges and corners of the specimen [71].

Figure 3.b shows the response of the FFF-printed cubic frame to external illumination with an intensity of 87 $mW.cm^{-2}$. The specimens are made from thermoplastic polyurethane (TPU) with carbon black (CB) fillers. Under light stimulus, the cubic parts could recover their original shape within 160 s. **Figure 3.c** depicts the shape recovery process of a 3D printed sample. The specimen was programmed beforehand: heated to its glass transition temperature of 190 °C, deformed, then cooled down to fix its shape. When heated again above its glass transition temperature, the flower bloomed within 30 s.

3.2. Stereolithography

One of the most common forms of stereolithography (SLA) is photo-polymerization. It consists of concentrating a light beam, most of the time a UV laser, in a tank filled with photopolymer, a synthetic resin whose molecules are cross-linked under the effect of ultraviolet light to form a solid-state [47]. Thus, the laser moves and solidifies the material on the surface, creating the first layer. The platform supporting the tray descends vertically so that the laser solidifies the next layer, and so on, until the final model is obtained [56].

Several manufacturing parameters influence the quality of the product printed by the SLA process. According to Alharbi et al. [72], the compressive behavior depends on the printing orientation. The tested parts were made from a commercial resin for dental implants. The specimens printed along the vertical direction exhibited more compressive strength (297 MPa) than those printed horizontally (257 MPa). Arnold et al.[73] assessed the effect of the layer thickness and the printing orientation on surface roughness. They tested samples made from polyurethane (PU) destined for dental implants. The authors determined that the optimal surface quality (roughness equal to 0.87 µm) is obtained with a layer thickness of 100 µm and a 15° printing orientation. Also, Hada et al. [74] investigated the effect of printing direction on the dimensional accuracy of SLA printed dental implants. Three sets of samples were created with different printing directions: 0°, 45° and 90°. The 45° specimens exhibited the best geometrical accuracy with root mean square error equal to 0.05 mm.

Cekic et al. [75] investigated the relation between SLA process parameters and the dimensional accuracy of manufactured parts. The authors observed that the quality surface is better for lower printing speeds and thinner layer thicknesses. They concluded that, for optimal surface quality, the thickness height should be set to 0.1 mm and the printing speed should range between 50 $mm.s^{-1}$ and 100 $mm.s^{-1}$.

Zhao et al. [76] studied the mechanical and shape memory properties of synthesized polyurethane acrylate photopolymer (PUA). The test specimens were printed via the SLA process. They showed high dimensional accuracy and high shape memory performance: the shape fixity ratio is 96.77%, the recovery ratio is 100% and the recovery stress is 6.4 MPa.

Seo et al. [77] investigated the behavior of temperature-responsive hydroxybutyl methacrylated chitosan (HBC-MA). The specimens were printed with SLA technique and they were intended to imitate the dynamic behavior of biological tissue. At low temperature (10 °C) the structure's volume increases (swelling ratio of 7.16) due to water expansion in the polymer. And reversibly, its volume decreases when the temperature rises. The compression behavior of the printed tissue

exhibited a temperature dependence. The compression modulus was equal to 219.57 kPa at 10 °C and 543.91 kPa at 37 °C.

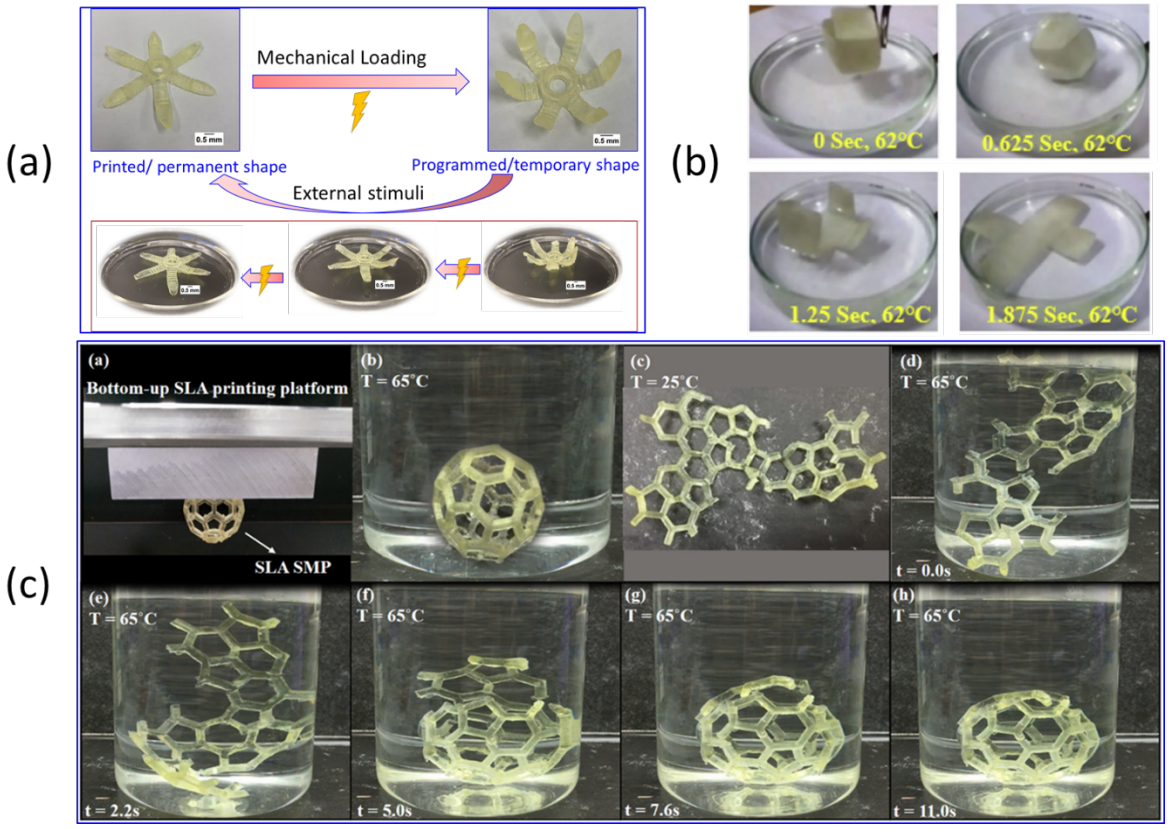

Figure 4. SLA printed parts using shape memory materials: **a.** Shape memory behavior of smart grippers. Reproduced with permission. [78] Copyright 2021, Elsevier. **b.** Unfolding Cubical SMP sample. Reproduced with permission. [79] Copyright 2021, Wiley. and **c.** A complex SMP bucky ball. Reproduced with permission. [80] Copyright 2017, Elsevier.

Figure 4 shows parts printed with SLA technique: **Figure 4.a** shows the shape memory behavior of smart gripper made from a mixture of benzyl methacrylate (BMA), methacrylate poly (ethylene glycol) dimethacrylate (PEGDMA), and phenylbis (2,4,6-trimethyl benzoyl) phosphine oxide (BAPO). After being programmed to a temporary shape, the gripper regains its permanent form when placed in warm water. **Figure 4.b** showed the shape recovery of a cubical sample made from acrylated epoxidized soybean oil (AESO) when heated to 62 °C. **Figure 4.c** represents the shape memory behavior of a SMP Buckminsterfullerene (C60 bucky-ball). When immersed in a 65 °C water bath, the sample recovered its folded form in 11 s.

Shan et al. [81] used the SLA process to produce thermo-responsive shape memory polymer made by blending epoxy acrylate (EA) with isobornyl acrylate (IBOA) and trimethylolpropane triacrylate (TMPTA). The material has a melting temperature of around 300 °C. The SLA printed objects are characterized by high resolution and transparency with average transmittance equal to 95.6%. The specimens have an ultimate tensile stress of 26.4 MPa with an ultimate strain of 12.6%. The samples can recover their original form in just 6 seconds at 90 °C temperature. The material was tested as an electrical-responsive and temperature-responsive actuator for electronic devices applications.

Choong et al. [82] developed and investigated the durability of an SLA printable *tert*-butyl acrylate (tBA) polymer. The printed specimens' elastic modulus, tensile strength and maximum elongation are 230 MPa, 20.2 MPa, and 8.79%, respectively, at a temperature lower than 54 °C. The samples were able to keep 100 % of their shape fixity and shape recovery ratios after 14 thermo-mechanical cycles. The advantages of this type of 3D printing are the printing accuracy, the excellent finish, the ability to print transparent parts and the large stiffness range from flexible to very stiff. Its disadvantages are problematic internal volumes, the fragility of materials, and the aging of parts: they display photosensitivity and hardening when exposed to ambient UV [4].

3.3. Digital Light Processing

Digital Light Processing (DLP) is a 3D printing technique that uses a light projector to cross-link oligomers tailored to photopolymerize. While an UV laser beam is used in SLA, a light source is used instead in the case of DLP printing. Objects are created in the same way as with the SLA process: the object can be pulled out of the tank filled with photopolymer, creating space at the bottom of the tank for the next layer, or it can be dipped into the tank to create a new layer on its surface [83].

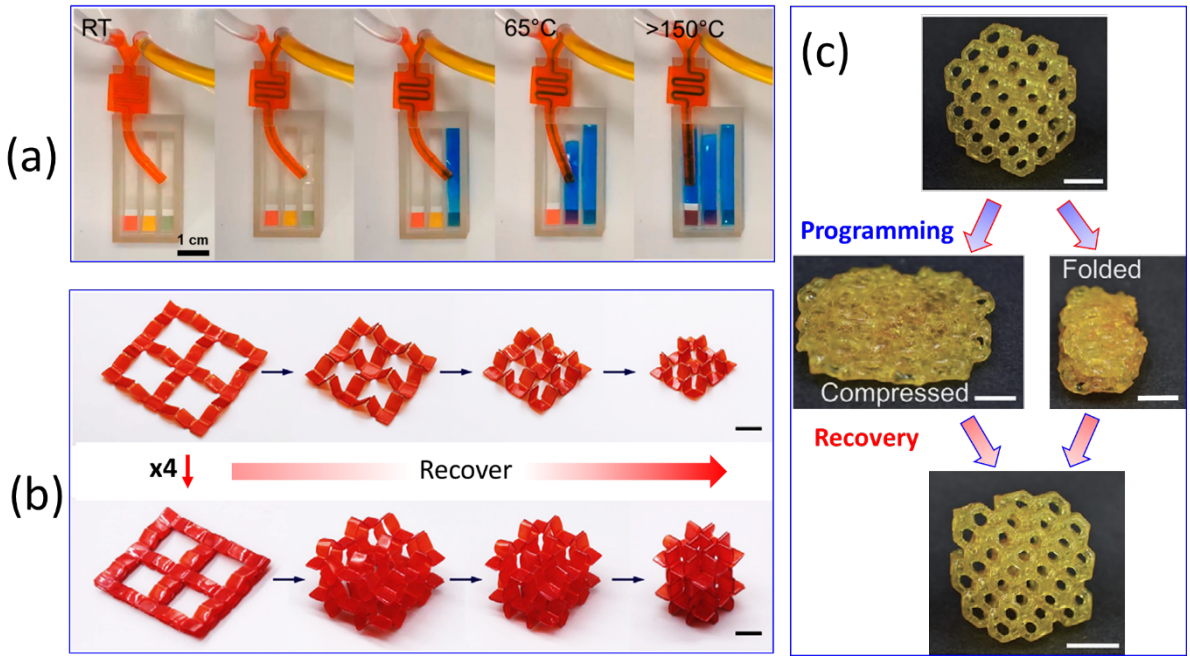

Figure 5. DLP printed parts with shape memory properties: a. Microfluidic device. Reproduced with permission. [84] Copyright 2019, American Chemical Society. (b) Single-layer and multi-layer lattice structures. Reproduced with permission. [85] Copyright (2020), with permission from Elsevier. and (c) Grid pattern foam. Reproduced with permission. [86] Copyright 2021 Wiley.

Figure 5 shows different parts printed with the DLP technique. **Figure 5.a** shows a heat-responsive microfluidic device made from a mixture of poly (ethylene glycol) dimethacrylate (PEGDMA), IBoA, and 2-ethylhexyl acrylate (EHA). When the temperature increases between room temperature and above 150 °C, the shape of the device changes and it allows the filling of another location. **Figure 5.b** shows the evolution of single-layer and multi-layer lattice films from 2D to 3D structures under heat-stimulus. **Figure 5.c** demonstrates the behavior of shape-memory Kelvin foam. After being compressed or folded, the printed parts recover their original form when heated to 80 °C. This cycle can be repeated more than 10 000 times.

The DLP technique can execute the whole pattern of one layer in a single exposure, making it more efficient than the SLA technique. In addition, it can produce high resolution at micro and nanoscales [87].

The objects printed by this process have relatively the same characteristics as the SLA printed ones. However, they both have smoother surfaces than other techniques such as FFF [88]. Compared to SLA, DLP is faster and less expensive. Indeed, this process does not involve any movement of the light on the horizontal axis, unlike the UV laser of the SLA process, which must scan the tank point by point to trace each slice of the object, only the platform is gradually lowered [56].

Several researchers studied different aspects of the DLP technique. Chen et al. [89] developed a hybrid ink by mixing an acrylate resin made from 2-Hydroxyethyl acrylate (HEA), IBOA, and trimethylolpropane ethoxylate triacrylate (TMPTA) with a thermally curable epoxy resin made from diglycidyl ether of bisphenol A (DGEBA) and methyl tetrahydrophthalic anhydride (MTHPA). The specimens made from the combination of the two polymers exhibited better mechanical characteristics than those made from only one of each polymer. The elastic modulus and strength increased to 2.59 GPa and 59.2 MPa, respectively. The polymer blend has a glass transition temperature of approximately 95 °C. The non-polymerized ink remaining in the tank was then recycled and reused. The reprinted specimens showed a relatively small decrease in the elastic modulus and strength to 1.55 GPa and 37.8 MPa, respectively. Cortés et al. [90] developed a DLP printable SMC composed from poly(ethylene glycol) diacrylate/poly(hydroxyethyl methacrylate) matrix reinforced with multi-walled carbon nanotubes (CNTs). The printed parts are electro-responsive, and the Joule effect triggered their shape recovery. The electrical conductivity increases as the CNT's volume fraction increases. It is equal to 5.8 10^{-1} $S.cm^{-1}$ for 0.5 wt.% of CNTs. The samples exhibited high shape memory performances. The shape fixity ratio and the shape recovery ratio are equals to 100% and 95%, respectively. Peng et al. [84] created an ink made from acrylic comonomers for DLP printing. Two glass transition temperatures characterize the new material. The first one is between -8 °C and 51 °C. The second one ranges between 88 °C and 110 °C depending on the volume ratios of each material's constituents. This property allows the material to have a multi-shape effect.

The shape fixity and the shape recovery ratios of the printed samples are above 90%. The printed specimens were also tested as microfluidic devices. Wu et al. [91] made a new shape memory polymer from tBA/1, 6-hexanediol diacrylate (HDDA) networks. The material is used as an ink for the DLP printing process. The crosslinker weight ratio has a significant influence on the shape memory properties. The testing results showed that the printed parts with 10 wt% of HDDA kept a 100% shape recovery ratio after 14 cycles. The ones with 20 wt% have a higher shape fixity ratio equal to 95%. The glass transition temperature ranged from 48.7 °C (10wt% of HDDA) to 76.3 °C (50 wt% of HDDA).

4. Shape memory polymeric materials

Moving from three to four dimensions requires several factors as explained in **Figure 6**: the use of intelligent materials that react to an external stimulus; the presence of this stimulus (change of temperature, hygrometry, magnetic field, etc.); an interaction between the material and the stimulus (change of shape by absorption of water, for example); and the contribution of mathematical modelling, in order to conceive the distribution and the functionalities of the material, and to predict and program its future evolution.

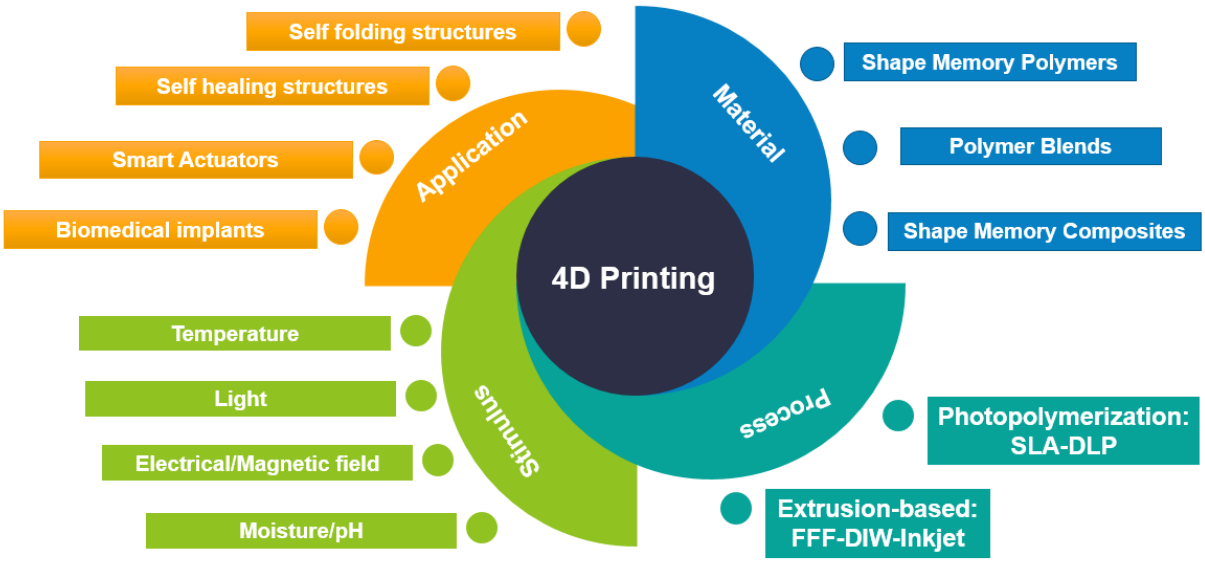

Figure 6. 4D printing parameters and environment

Today, shape-memory materials are capable of "remembering" a state. This memorization involves at least two steps: applying a stimulus causes the object to change from its original form to a temporary state, which it retains until a second stimulus causes it to return to its original form. Once modified, this structure can then return to this temporary state, spontaneously or by programming, which is infinite since the process is reversible [92].

Applications of 4D printing in soft robotics, smart textiles, drug delivery, and regenerative medicine are being considered [27, 93]. Stimuli-responsive programmed material systems offer an alternative to complex electromechanical devices.

4.1. Shape memory concept

To ensure the shape memory effect, the presence of two distinct phases with different mechanical properties is necessary [43]. A first ductile phase ensures the deformation and the passage towards the transitional shape. A second one, a less ductile phase, ensures the return to the initial state. These phases are called "switching domains." The physical and chemical interactions between the two phases drive the evolution of the shape during the programming. The stimulation makes the ductile phases more flexible and ensures the changes [41].

In the case of thermosetting polymers and elastomers, a single polymer has both functions to ensure the shape memory effect because they have two different phases, hard segments (HS) and soft segments (SS). In the case of thermoplastics, at least two polymers and/or copolymers are often necessary to form the blends [94].

The phases formed by the rigid segments have a higher transition temperature, while the domains ensuring the form changes (soft or switch segments) have a lower transition temperature than the hard segments. The thermal transitions are the glass transition temperature (T_g) and melting temperature (T_m). All polymers exhibit a glass transition temperature associated with the mobility of macromolecular chains of the amorphous phase, whereas only semi-crystalline thermoplastics have a melting temperature. The glass transition and the melting transition extend over a wide range of temperatures as shown in **Table 3**. The hardening of the

polymer chains at the molecular level allows a temporary fixation of the shape of the SMP. During the cooling of the sample to a lower temperature than the processing temperature, the phase that ensures the deformation solidifies and loses flexibility [95]. Thus, the chains are oriented in an energetically non-stable state. Heating the sample lets the ductile phase get back to moving chains and get back into balance [96].

Table 3. Glass transition temperatures and melting points of some SMPs.

SMP	PTMO	PPG	PU	PCL	PP	PVA	PLA	PET	PTFE	PMMA	PC
Tg [°C]	-84	-75	-63	-60	-13	30-45	50-80	72	117	125	174
Tm [°C]	23-28	-40	57	60	135-165	60	175	260	327	-	243

Shape memory polymers have two types of behavior: one-way shape memory polymers and two-way polymers [94]. One-way shape memory polymers always return to their initial shape after deformation [97]. Under the influence of an external stimulus, they can change and temporarily fix a new shape, which is stable over time. The permanent shape is recovered under the application of the same stimulus [98]. As for the two-way shape memory polymers, they can gradually change their shape under the effect of a stimulus [99]. However, when this stimulus is no longer applied, the polymer immediately returns to its initial shape. Thus, unlike the one-way shape memory polymer, this type of polymer does not have a stable temporary shape [100]. Two-way shape memory polymers do not necessarily require human intervention to be programmed which allows them to be used in continuous cycles [101].

Thermoplastics can be returned to a malleable state repeatedly by heating them. This ability stems from the reversibility of weak bonds such as hydrogen and van der Waals bonds with temperature. When the thermoplastics are heated, the weak bonds retaining the macromolecules break up, allowing the latter to be free to move, resulting in the softening of the polymer. Upon cooling, the weak bonds are recreated and the material returns hard. The effect of heat thus

shapes them. Their interest arises from their recyclability and lower environmental impact than thermosets. ABS and PLA are the most commonly used for additive manufacturing [102].

Elastomers are a particular type of polymer. They have a glass transition temperature lower than 0 °C. They are characterized by an amorphous structure with a low cross-linking density, which gives a low elastic modulus, good ductility, and high failure strain [103].

The elastomers have the advantage of a rapid shape recovery process thanks to their high elasticity [104]. Similar to other polymers, they can also be combined with fillers and additives to form composite materials [105] or be used in multi-material parts to form self-actuating structures [106]. Shirole et al. [11] mixed electrospun poly (vinyl alcohol) (PVA) fibers with polyether block amide elastomer (PEBA). PVA provided the shape memory properties for the material. Specimens containing a higher percentage of PVA showed a better recovery ratio and shape fixity. Other SMPs were created with the same method. These materials are degradable, which gives them the potential to be applied in biomedical fields [107, 108]. Raasch et al. [109] compared the thermomechanical properties of 3D printed parts with and without heat treatment. Annealing treatment at different temperatures affects tensile and shape memory properties. The glass transition temperature of annealed parts is 41.5 °C compared to 51.9 °C of non-treated ones. The ultimate tensile strength at 25 °C of annealed samples is 34.1 MPa which is lower than the non-treated ones that is equal to 49.8 MPa. However, at 70 °C the tensile strength of heat-treated specimens is higher that the non-annealed ones (3.5 MPa vs. 0.18 MPa). The Young modulus is lower for the annealed specimens at 25 °C (0.6 GPa vs. 1.99 GPa) but higher at 70 °C (0.009 GPa vs. 0.002 GPa). The recovery ratio was better for the annealed samples. The heat treatment temperature has an impact on the shape recovery ratio: specimens annealed at 85 °C have the highest ratio of 98.7 % after 1000 s.

4.2. Polymer blends

A shape memory polymer is usually combined with another to obtain improved mechanical characteristics, new shape memory properties or to create a new material in which one polymer

is the fixing phase while the other is the reversible phase [110]. Thermoplastics, elastomers and thermosets, can be blended to bring additional functionalities such as multi-shape memory effect, self-healing and multi-stimuli responsiveness. Various techniques, such as electrospinning, melt mixing, solid-state foaming or interpenetrating polymer networks, can be used for producing polymer blends [111].

Figure 7. represents the range of glass transition temperatures and melting points of the most commonly used SMPs in additive manufacturing. For amorphous thermoplastics such as PMMA, a softening temperature is used instead of Tm in the graph. Glass transition temperatures vary from -80 °C for PTMO to 170 °C for PC. While for melting points, the variation ranges from -40 °C for PPG to 330 °C for PTFE. Materials can be classified into two groups: the first one with close T_g and T_m, like PPG, PVA and PCL and the second one with higher disparity between T_g and T_m, like PP, PET or PMMA, for example.

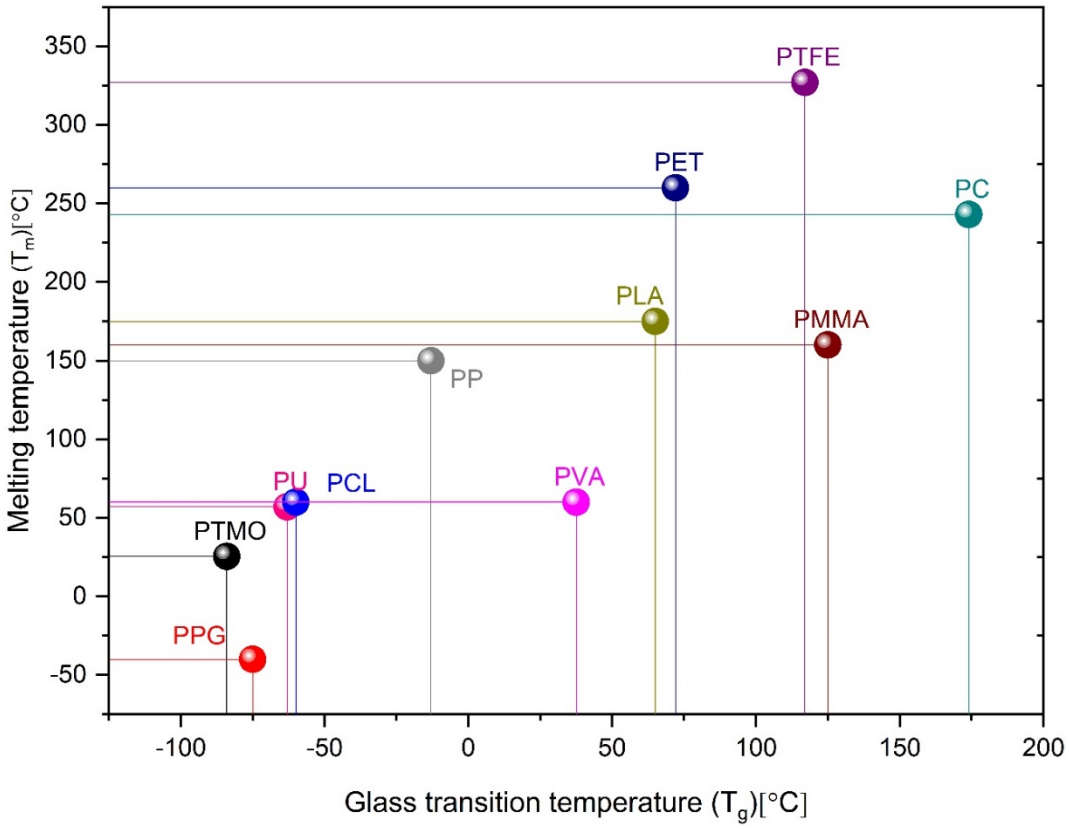

Figure 7. Glass transition temperatures and melting points of some SMPs

Song et al. [112] mixed different weight ratios of TPU and PLA polymers to form a new shape memory blend. Two glass transition temperatures characterize the new material: the first one is comprised between 60 °C and 62 °C while the second one ranges between-34.8 °C and -38.9 °C. They evaluated different weight fraction combinations. The microstructure of the polymer blends showed immiscibility even though the mixed polymers are considered compatible and have isotropic properties. The porous morphology of the material is linked to the weight ratios of the components. For example, the specimens with 80/20 TPU/PLA blend had lower pore size (0.23 μm) and higher pore density (6.1010 pores per cm3). However, they showed similar shape memory behavior and were uniformly contractible when exposed to heat.

In **Table 4,** we summarize some of the most common shape memory blends in the literature: their composition, the stimuli to which they respond, their compatibility with 3D processes, as well as their mechanical and shape memory properties.

4.2.1. Polymer blends in SLA

The fundamental principle of producing the shape memory effect in SLA polymers is to combine softer components with stiffer ones. The structure of photopolymerized crosslinked thermosets is rigid and dense, which reduces the spaces between molecular chains and disables them from moving. That is why these kinds of polymers have fewer good SME properties [110]. Multiple researchers study SLA-printable SMP blends. Wallin et al. [113] developed an SLA printable SMP blends of two different elastomers: mercaptosiloxane (MS) and vinylsiloxane (VS). The polymeric blends can be 3D produced using a standard SLA printer with low energy. The thermo-mechanical properties of the printed specimens can be controlled by varying the volume fraction of the polymer's components. The elastic moduli and ultimate stresses range between 6 kPa and 287 kPa and between 13 kPa, and 129 kPa, respectively, depending on the blends' composition. The samples exhibited an ultimate elongation of up to 138.75%. Kim et al. [114] created SLA printed polyvinylidene fluoride (PVDF)-based blends. The polymer to solvent ratio is optimized to obtain the best printability and piezoelectric properties. The

specimens can generate up to ±0.180 nA when subjected to an 80 N tensile force and have a piezoelectric coefficient equal to 0.014 pC/N. Zhao et al.[78] designed a shape memory blend for the SLA printing process. The ink is a mixture of BMA, PEGDMA and BAPO. The printed parts consist of heat-responsive grippers. Their shape memory recovery is triggered when put in a water bath with controlled temperature. The experimental results as well as the analytical model developed by the authors determined that when thermomechanical cycles increase the shape fixity of the material drops while the shape recovery ratio increases. In addition, the printing parameters significantly influence the behavior of the printed parts. For instance, higher scanning speed leads to faster decay of the material.

Table 4. 4D printable SMP and blends' properties

SMPs	Stimulus	DoE factors	AM process	Blend's characteristics	Ref
Triallyisocyanurate (TAIC) + PLA	Heat	*Monomers ratio *Irradiation temperature *Printing direction	FFF	*Ultimate stress: between 7.31 MPa and 49.9 MPa depending on irradiation temperature and printing direction. *Ultimate strain: between 7% and 24% depending on irradiation temperature and printing direction. *Failure stress: between 6.73 MPa and 40.1 MPa depending on irradiation temperature and printing direction. *Failure strain: between 7% and 24% depending on irradiation temperature and printing direction. * T_g: ~ 35 °C	[115]
Benzophenone (BP) /PLA/Dichloromethane (DCM)	Heat	*Contents weight ratio *Parts geometries	3DP	*Elastic modulus: 1440 MPa *Maximum strength: 43 MPa *Strength at break 32: MPa *Elongation at break: 203,5% *Shape recovery ratio: 99,02% * T_g: 66 °C	[116]
BMA+ Poly (ethylene	Heat	*DEGDMA and BMA weight ratios	projection	* Maximum strain: ~ 330% (at 40 °C)	[117]

glycol) dimethacrylate (PEGDMA) + Bisphenol A ethoxylate dimethacrylate (BPA) +Di(ethylene glycol) dimethacrylate (DEGDMA)			micro-stereolithography (PμSL)	* Shape fixity: > 90% when the temperature is above or near Tg. *Shape recovery ratio: >95% * Rubbery modulus: up to 79.45 MPa depending on the components weight ratio. * T_g: from ~ − 50 °C to ~ 180 °C depending on BPA, DEGDMA and BMA weight ratios *Ultimate stress: around 37 MPa (At 25 °C) *Qualitatively: the material has typical elastic-plastic behavior with low fracture strain (At 25 °C)	
VeroWhitePlus© (Photopolymer) + TangoBlackPlus© (liquid resin) (Stratasys Trademark)	Heat	*Components weight ratio	3DP	*Recovery rate: between 97% and 99% *T_g: between 47.4 °C and 55.6 °C depending on the components weight ratio.	[118, 119]
Styrene-b-(ethylene-cobutylene)-b-styrene (SEBS)+ polyethylene wax (PEW)+ low density polyethylene (LDPE)	Heat	*Components weight ratio	FFF	*Shape recovery ratio and shape fixing ratio: up to 100% depending on the blend's components weight ratio and testing conditions.	[120]
PCL+ 2-ureido-4[1H]-pyrimidinone (UPy)	Heat	* UPy weight ratio *Healing process	DLP	* Elastic modulus: between 170 MPa and 190 MPa *Shape recovery ratio: between 24.8% and 100% depending on UPy weight ratio * Healing efficiency: up to 53.6% * Maximum tensile strength: ~ 12.5 MPa	[121]

TPU + aniline trimer (AT)	Heat	*Components weight ratio *Printing orientations	DIW	* Elongation at break: between ~225% and ~280% depending on testing conditions *Elongation at break: up to 295.1% *Tensile strength: up to 22.5 MPa *Healing efficiency: 92% (1st healing test) and ~72% (5th healing test) * T_m: 42.8 °C and 44.9 °C depending on the components weight ratio. *Shape fixing ratio: >90% *Shape recovery ratio: > 90%	[122]
1,4-bis-[4-(6-acryloyloxhexyloxy)benzoyloxy]-2-methylbenzene (RM82)+ n-butylamine+ Photoinitiator Irgacure I369	Heat	*Parts geometry *Printing orientations	DIW	*Elastic modulus: between 4 MPa and 18 MPa depending on printing orientation.	[123]
1,4-Bis-[4-(6-acryloyloxyhexyloxy)benzoyloxy]-2-methylbenzene+ n-butylamine+ Irgacure 651	Heat	*Ink composition *Printing parameters *Ink rheology	DIW	*Elastic modulus: 3.1 MPa *Parts keep their shape memory behavior after 100 cycles *Storage modulus: up to ~ 7.10^5 Pa *Supporting weight: ~106 g *Recovery time: (full cycle) ~ 390 s *T_g: -22 °C	[124]

Liquid crystal mesogen RM257+2,2'-(ethylenedioxy) diethanethiol (EDDET) + photo initiator (Irgacure 2959)	Heat	*Printing parameters *Parts geometry	DIW	*Maximum actuation strain: ~20% (depending on printing temperature and printing speed) * Poisson's ratio: < 0 (at room temperature) * Poisson's ratio: > 0 (at room temperature) *T_g: Between -24.3 °C and 48.8 °C	[125]
tBA+ di(ethyleneglycol) diacrylate (DEGDA)	Light	*Photoinitiator (PI) weight fraction *DEGDA weight fraction	SLA	*Tensile Strength: 20.2 MPa ($T<T_g$) and 0.3 MPa (at Tg) * Elastic Modulus: 230 MPa ($T<T_g$) and 1.66 MPa (at Tg) * Elongation at break: 8,79% ($T<T_g$) and 18.2% (at T_g) *Shape fixity: between 84.9% and 95.2% depending on DEGDA weight fraction *Shape recovery: between 97% and 99% depending on DEGDA weight fraction * T_g: 53.9 °C (When DEGDA 10 wt%)	[82]
PUA + 1-hydroxycyclohexyl phenyl ketone (PI184) + Bisphenol A diglycidyl ether diacrylate (DGEDA)+ IBOA	Light	*Parts geometry *Temperature effect	SLA	* Glass modulus: 1820.2 MPa (at 25 °C) * Rubbery modulus: 7.2 MPa (140 °C) *Recovery time: between 18 s and 8.5 s depending on temperature * Tensile strength: 37.3 MPa (at room temperature)	[76]

				*Elongation at break: 24.8% (at room temperature) * Elastic modulus: 1267.1 MPa * Average shape fixity ratio: 96.77% (16 cycles) *Average shape recovery ratio: 100% (16 cycles) * T_g: 92 °C	
Soybean oil epoxidized acrylate+ bis(2,4,6-trimethylbenzoyl)-phenylphosphineoxide	Light	*Printing parameters: laser frequency and printing speed.	SLA	*Shape fixity: between 92% and 99% depending on laser frequency *Shape recovery ratio: 100% *Compression modulus: around 550 MPa for different laser frequencies. *T_g: 20 °C	[126]
poly(ethylene glycol) diacrylate (PEGDA) + 1-[4-(2-hydroxyethoxy)phenyl]-2-hydroxy-2-methyl-1-propanone-1-one photoinitiator	Electricity	*Parts geometry *Printing parameters *Temperature	SLA	*Elastic modulus: up to 741.6 kPa *Electrical resistance: up to 250 Ohm * Electrical conductivity: around 15.8 $mS.cm^{-1}$	[127]
Pluronic F127+aniline tetramer-grafted-polyethylenimine (AT-PEI)	Electricity	*Contents volume ratios	3DP	*Conductivity: > 2.0 × 10^{-3} $S.cm^{-1}$ *No Cytotoxicity *Loss modulus: around 1.4 kPa *Storage modulus: around 14 kPa	[128]

Sodium alginate + Pluronic F127 diacrylate (F127DA) macromer + $Ca2^{+}$	Chemical reaction	* F127DA weight ratio * Alginate weight ratio	3D bioprinting	*Maximum expansion rate: 377.5% * Fixity ratio: up to 89.34% * Recovery ratio: up to 99.07% * Cell viability: > 95% (after testing hydrogel as drug delivery system) * Biodegradibility: 85% of material remained after 7 days	[129]
Vinyl Caprolactam + polyethylene (PE) + Epoxy diacrylate oligomer + Iragcure 819	Humidity	*Parts geometry *Crosslinking density	Polyjet	*Expansion: 200% * Elastic modulus: 40 MPa (dry state) and 5 MPa (fully expanded state) *Poisson's ratio: 0.5 * Mechanical strength: 10.84 MPa	[130]
Collagen+ heparin sulphate+ acetic acid	pH	*Implants' material composition tested on lab rats	3D bioprinting	*Triggering pH value: ~7 *Compressive modulus: 3.46 MPa *Compressive strength: 308.9 kPa *Biocompatibility: allow cell regeneration	[131]
Keratin+ phosphate-buffered saline (PBS)+ riboflavin+ sodium persulfate (SPS)	pH	* Keratin volume fraction	DLP	* Compressive modulus: up to 15.45 kPa * Storage modulus: up to 12.8 kPa * Loss modulus: up to 4 kPa	[132]

4.2.2. Polymer blends in FFF

In contrast to photopolymerization and powder-based AM techniques, the extrusion-based techniques are compatible with a wide range of commercially available thermoplastics. Most of them satisfy all printing requirements and are moderately priced compared to other AM techniques [133]. The most commonly used materials for FFF, especially those for low-cost 3D printers, are mainly limited to PLA and ABS due to their ease of processing [134]. Recently, alternative materials have increased significantly, leading to various commercially available thermoplastics [65, 135]. Other polymers, even commercially available ones, often require a great deal of practical experience. Therefore, they still need processability, stability, and accuracy improvements, as shown for various types of studied filaments [136, 137]. The main success factor is their low coefficient of thermal expansion, which facilitates their processability, especially in terms of shrinkage, deformation, and distortion. However, most amorphous filaments reveal low toughness, a tight processing temperature range, and very low chemical resistance [138].

There is also research on unconventional materials to integrate them into this type of AM process, such as biopolymers [139, 140], silicone elastomers [141], recycled polymers [141-143], or highly filled polymers for the production of metals/ceramics parts [144, 145].

5. Shape Memory Composites

The basic definition of a composite material is an assembly of two or more immiscible materials of different natures. The resulting properties are a synergetic effect from the combination of each component taken separately. In general, a composite material consists of one or more discontinuous phases, called reinforcement, distributed into a continuous phase called the matrix [146]. Pure polymers have a low elastic modulus. Reinforcement such as fibers or particles enhances the overall material's behavior and properties, hence, extending its use for practical applications. Materials added to form a composite can be particles [147], short fibers [148], long fibers [149] or fabric [150]. Composite materials are often used to improve the properties of the finished product, such as tensile strength, density, and stiffness [151], or to add more

functionalities to the material. As with pure polymers, 3D printing of composites is strongly influenced by the printing parameters. The most influential parameters are printing orientation [24], layer height, and printing path [152].

The following section will review the effect of reinforcements on the materials' thermo-mechanical and shape memory properties.

5.1. Short and long fibers reinforcements

Typical fibers are made of glass, carbon, or polyaramid, namely Kevlar®. They are characterized by high elastic moduli and mechanical resistance, strengthening the shape memory polymer and enhancing its applicability [153]. Various methods can be used to reinforce SMP with fibers. For instance, Zeng et al. [154] developed a system where the PLA filaments and the continuous carbon fibers are extruded from separate customized feed channels before getting mixed, as illustrated in **Figure 8.a**. The material is then extruded from the main nozzle in laminate-form specimens. Dong et al. [152] used a modified printer to produce shape memory composite parts made from PLA matrix reinforced with Kevlar continuous fibers, as shown in **Figure 8.b**. At the same time, the feeding system can extrude the thermoplastic SMP filament and the continuous fibers through the printer's nozzle. Lin et al.[155] used a PBS/PLA composite to print parts with different geometries via the FFF process. The PBS and PLA pellets are simultaneously introduced to a feeder before being mixed in a melting system. The composite filaments are then extruded and winded to be used by the FFF printer, as illustrated in **Figure 8.c**.

The reinforcement of printable filaments follows two strategies. The first one is the addition of short fibers to improve mechanical performance, reduce warpage during printing and increase dimensional stability. The second one is the addition of continuous fibers, which enhance the mechanical strength [148]. 3D printing parts made of composites with either short or long fibers have many advantages over parts made of pure polymers [156]. Carneiro et al. [157] showed that adding 17.6% volume of glass fibers to PP leads to a 30% and 40% increase in elastic modulus

and tensile strength, respectively. In the same context, Love et al. [158] found that the addition of 8% volume of carbon fibers to an ABS matrix resulted in an increase in tensile modulus (+630%) and stress at break (+144%).

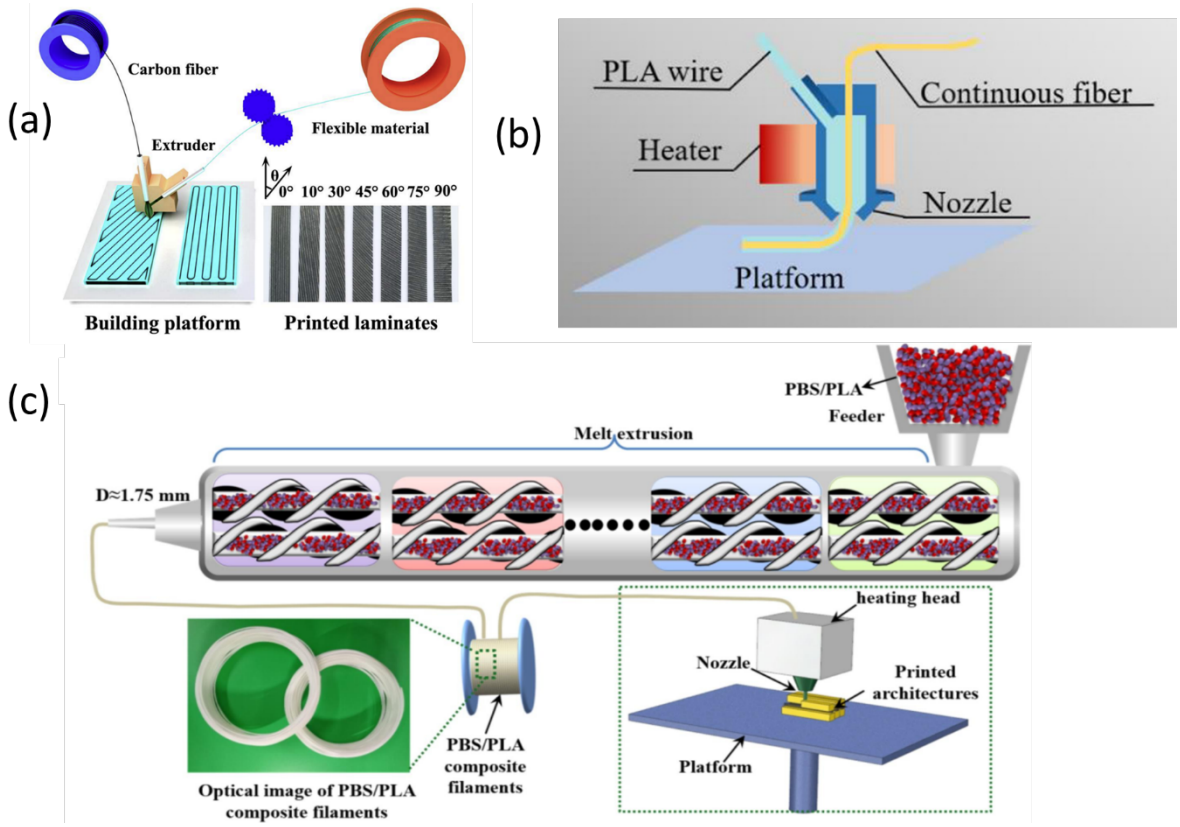

Figure 8. (a) Fabrication of fiber reinforced SMP laminates. Reproduced with permission. [154] Copyright 2020, Elsevier. (b) Continuous Kevlar fiber reinforced shape memory composite. Reproduced with permission. [152] Copyright 2021, Elsevier. (c) Schematic preparation of PBS/PLA composite filaments for the FFF printing process. Reproduced with permission. [155] Copyright 2022, Elsevier.

Guo et al. [159] used short carbon fibers to form an SMC with better mechanical properties as an additive to trans-1, 4-polyisoprene (TPI). The tests on specimens with different carbon fiber weight fractions between 5% and 13% showed that the mechanical characteristics depend significantly on this parameter. Samples with a 7% wt of carbon fiber weight fraction exhibit higher strength, elastic modulus, and shape recovery ratio than the other weight fractions.

Sun et al. [160] added elastic fibers composed of 20% of Spandex® and 80% of Nylon to styrene-based resin to form an SMC. The mechanical properties such as the elastic modulus, toughness, and tear strength were all improved. No significant change in shape memory characteristics was observed. The overall SMC properties allow it to be potentially used as a morphing skin in aeronautics.

Rahman et al. [161] investigated the effect of reinforcing the SMP polyurethane matrix with glass fibers. Different fiber volume fractions between 5% and 30% were analysed. While the mechanical behavior seems to be enhanced with the increase in glass fiber volume; the material loses its shape memory properties. As the material's stiffness went up, the mobility at the molecular level became less and less.

Xin et al. [162] used carbon fiber plain woven fabrics as an additive to overcome the lack of insufficient mechanical properties of pure styrene SMP. The mechanical analysis showed better storage modulus for the composite while the shape recovery ratio dropped steeply in temperatures under the glass transition temperature. The SMC was tested as a deployable solar actuated prototype and gave encouraging results.

In **Table 5,** we summarize some of the most commonly used shape memory composites in the literature: the SMPs and additives used, the stimuli to which they respond, the 3D processes with which they are printed, as well as their mechanical and shape memory properties.

5.2. Nanomaterials' reinforcements

Nanocomposites are, by definition, made of at least two materials, one of which has one dimension less than 100 nm [163]. Nanomaterials can be added to SMPs in different shapes: fibrous, layered or spherical [42].

As additives, nanomaterials have the advantage of enhancing the mechanical properties of the composite like the elastic moduli and strength [164] by just adding low percentages (as low as 1.7% [165]), which improve the functionality of the composite material.

Table 5. Printable SMC and their characteristics

Matrix	Additives	Stimulus	AM process	DoE factors	Material Characteristics: mechanical and shape memory properties	Reference
Semicrystalline PCL + Aliphatic urethane diacrylate (AUD) + n-butyl acrylate (BA)	Silica nanoparticles Volume fraction: 4% Length: between 200 nm and 300 nm	Heat	DIW	*Parts geometry *Printing orientation	* Maximum strain: up to 300% * Fracture strain: 500-600% * Elastic Modulus: up to 7.8 MPa. * Shape fixity (R_f): over 93% (at 230% programming strain) * Shape recovery ratio (R_r): over 95% (1st cycle at 230% programming strain)	[24]
PLA Tg=62 °C Density = 1240 kg/m3, Tensile strength 65MPa, Breaking elongation 8%	Kevlar fiber Diameter: 0.025 μm, Breaking strength: 225.30 N/tex Breaking elongation: 3%	Heat	FFF	* Layer thickness * Cell length	*Elastic modulus: between 1151.11 MPa and 1434.83 MPa depending on cell length * R_r: up to 86.54% depending on cell length	[152]
Polydimethylsiloxane (PDMS)	Microspheres SiO_2 gas	Heat	DIW	*Glass transition temperature of SiO_2 microspheres (44 °C and 113 °C) * SiO_2 volume fraction	*Storage modulus: up to 10^6 Pa depending on SiO_2 glass transition temperature * Shape recovery ratio: highly dependent on Gas glass temperature, gas volume fraction and heat treatment	[166]
BA/DGEBA	SiO_2 nanoparticles	Heat	DIW	*Printing orientation *SiO2 weight ratio	*Shape fixity ratio: 97.1% *Shape recovery ratio: 98.5% *Elastic modulus: 0.82GPa *Ultimate strain: up to 25.4%	[167]

					All depending on SiO_2 and photopolymer weight fractions.	
PU-based polymers	Multi-walled carbon nanotubes (MWCNTs) Length: between 100 µm and 200 µm Average Diameter = 8 nm	Heat	FFF	*Parts' geometry *Environment temperature *Printing parameters (temperature, layer thickness, feed rate)	*Electrical resistance: between 1.09 and 2.27 kOhm *Restoring time: between 42 s and 230 s (Depending on printing parameters and mainly the layer thickness) *Glass transition temperature: 35 °C.	[55]
PU/ polyethylene oxide (PEO) PU/gelatin	Iron oxide nanoparticles (SPIO NPs) Length : < 20 nm	Heat	3DP	*Ink composition	*Storage modulus: 320 kPa *Shape fixity: ~100% (50 °C) *Shape recovery: ~75% (50 °C) *Storage modulus: 227 kPa *Shape fixity: ~95% (50 °C) *Shape recovery: ~85% (50 °C)	[168, 169]
VeroBlack (Thermoset acrylic resin)	TangoPlus (Thermoplastic-like elastomer)	Heat	3DP	* Components weight ratio * Material layout	* Shape fixity: between 10% and 90% (depending on material layout and the components volume fraction).	[170]
PU+ Sodium chloride (NaCl)	Tungsten (purity > 99.9%, 0.6-1 µm)	Heat	FFF	*Parts geometry *Tungsten addition *NaCl weight ratio	* Shape recovery: up to 100%. * Maximum storage modulus: 926 MPa (at -10 °C) *T_g: 31.4 °C	[171]
PU+ carboxymethyl cellulose (CMC)	*Silicon oxide (SiO_2) nanoparticles	Heat	FFF	* SiO_2 or CMC weight ratio * SiO_2 or CMC addition	*Elastic modulus: up to 10 MPa depending on SiO_2 weight ratio	[172]

					* Elastic modulus: up to 12 MPa depending on CMC weight ratio *Fracture stains: 11% (for CMC) and 19% (for SiO_2) *Ultimate tensile strengths: 1.01 MPa (for CMC) and 1.89 MPa (for SiO_2) *T_g: ~121 °C	
TPU	PLA	Heat	FFF	* Printing parameters: printing speed, nozzle temperature, flow rate, and layer height. *Parts geometry	* Shape recovery rate: 100% (under 10 cycles) and <20% (after 70 cycles)	[173]
PU-based polymers	Nylon fabric plain-woven	Heat	FFF	*Layer thickness	* Shape recovery ratio: 100% (up to 50 cycles) *Response time: between 1.8 s and 37.1 s depending on layer thickness *Elastic modulus: between 14.7 MPa and 209.2 MPa depending mainly on layer thickness and partially on the number of cycles	[174]
Epoxidized soybean oil (ESBO) + bisphenol F diglycidyl ether (BFDGE)	Carbon nanofibers (CNFs) Length = between 20 and 200 µm Diameter = 100 nm	Electricity/ heat	3DP	*Parts' geometries *Components weight ratio	*Electrical conductivity: ~0.4 $S.cm^{-1}$ *Storage modulus: 150 MPa and 300 MPa depending on CNF volume fraction *Rubbery modulus: between 3 MPa and 20 MPa at (150 °C) *Tg: highly dependent on ESBO/BFDGE weight ratio	[175]

PLA	Silvercoated carbon nanofibers (Ag@CNFs) Average thickness: 100 nm	Electricity	3DP	*Nozzle diameters *Solvent content *Material composition *Solvent evaporation	*Elastic modulus: between 1632 MPa and 2901 MPa depending on Ag@CNF volume fraction *Fracture strength: between 33 MPa and 54.9 MPa depending on Ag@CNF volume fraction *Elongation at break: between 2% and 17.3% depending on Ag@CNF volume fraction	[176]
D,L-lactide-co-trimethylene carbonate (PLMC)	CNT	Electricity	DIW	*CNT weight ratio *Parts geometries	*Electrical conductivity: between 65 Sm^{-1} and 106 Sm^{-1} *Elastic modulus: up to 1016.8 MPa *Tensile strength: up to 26.2 MPa * Elongation at break: 24.2% *Shape fixity: ~100% (after 4 cycles) *Shape recovery: ~100% (4 cycle)	[177]
PU-based polymers	CB nanoparticles	Electricity	3DP	*CB volume fraction *SMPC weight ratios	*Average elastic modulus: 160.26 MPa * Maximum strain: 44% (enhanced from 9.45% by adding CB)	[178]
BP/PLA/DCM	Fe_3O_4 nanoparticles	Magnetic Field	3DP	* Fe_3O_4 weight ratio *Parts geometries	*Elastic modulus: 1400 MPa *Maximum strength: 41.3 MPa *Strength at break: 34.53 MPa *Elongation at break: 32.4% *Shape recovery ratio: 95.14%	[116]

					*T_g: 71 °C	
PLA	Fe_3O_4	Magnetic Field	FFF	* Fe_3O_4 weight ratio *Parts geometries	*Mechanical strengths: up to 19.19MPa *Elastic modulus: up to 1293 MPa *Fracture strain: 27% (at 40 °C) *T_g: 65.35 °C and *T_m: 170.55 °C	[179]
PDMS/dibutyl phthalate/fumed silica	Microparticles of neodymium-iron-boron (NdFeB)	Magnetic Field	3DP	*Parts geometries	*Shape recovery ratio: 100% (after 1000 cycles) *Maximum compression stress loss: 8.3% after 1000 cycles *Maximum tensile stress loss: 13.3% after 1000 cycles *Poisson's ratio: 0.49	[180]
TPU	Magnetic Nd2Fe14B powder	Magnetic Field	SLS	*Magnetic powder weight ratios	* Maximum induction intensity: 50 mT * Tensile strength: between 14.53 MPa and 9.93 MPa depending on magnetic powder weight ratios * Elastic modulus: up to 70.53 MPa * Elongation at fracture: 89.5%	[181]
PLMC	Graphene oxide (g-GO) / silica nanoparticles	Light	3DP	* g-GO volume fraction	* T_g: between 37.8 to 42 °C depending on g-GO volume fraction * Shape recovery time: 8 s	[182]
PU	CB	Light	FFF	*Printing parameters * CB weight ratio	* T_g: 30 °C *Shape memory effect triggered by day light *Shape recovery ratio: 100% in ambient conditions	[62]

T**able 6** represents some of the used nanoparticles to reinforce SMPs, the stimulus used to activate the memory shape and their potential applications. A wide range of nanoparticles can be used to reinforce SMPs, such as metallic, ceramic or organic particles.

Table 6. Shape memory nanocomposites and their potential application

SMP	Nanoparticles	Stimulus	Potential Application	Refs
PCL / AUD / BA	Silica nanoparticles	Heat	Soft robotics, and biomedical devices	[24]
PLA	Kevlar nanofiber	Heat	Lightweight cellular composite	[152]
BA/ DGEBA	SiO2 nanoparticles	Heat	-	[167]
PU	CNT	Heat	-	[55]
PU/ PEO	Iron oxide nanoparticles	Heat	Magnetic carrier technology	[168]
PU/ CMC	SiO2 nanoparticles	Heat	Biomedical engineering, soft robotics	[172]
ESBO/ BFDGE	CNT	Electricity/ heat	Medical, aerospace, and robotic devices	[175]
PLA	Ag@CNFs	Electricity	Smart electrical devices in areas of soft robotics, sensors, wearable electronics	[176]
PLMC	CNT	Electricity	Liquid sensors	[177]
PU	CB nanoparticles	Electricity	Electrically conductive systems	[178]
BP/PLA/DCM	Fe3O4 nanoparticles	Magnetic Field	Soft robotics, flexible electronics, minimally invasive medicine	[116]
PLMC	Graphene oxide/ silica nanoparticles	Light	implants for bone tissue engineering applications	[182]

Leng et al. [183] compared the behaviors of light-responsive SMP before and after adding 10 wt% of nanocarbon particles as reinforcement. The test shows a better shape recovery speed for the nanocomposite due to its superior infrared light absorption and storage modulus.

Wei et al. [176] designed a new 3D printable nanocomposite material from conductive SMP matrix and silver-coated carbon nanofibers (Ag@CNFs). Two grams of Ag@CNFs were mixed with various quantities of PLA ranging from 0.5 to 4.67 g. The new material is characterized by its high conductivity equal to 2.1×10^5 $S.m^{-1}$ and its responsiveness to a low voltage equal to 1 V. These properties give it the potential to be used in electric triggered devices directly after printing since no post-treatment is required.

Silica nanoparticles can be added to SMPs to improve their properties [184]. Lee et al. [185] combined PU polymer with silica nanoparticles to create a shape memory material. The thermo-mechanical tests showed enhanced thermal stability and increased elastic modulus. The shape recovery effect was also improved. However, this was only observed when the nanoparticles' volume fraction was under 1%. Once it exceeded this threshold, all the mentioned properties began to degrade.

Auad et al. [186] used organic fibers (nanocellulose) to reinforce PU matrix to improve the mechanical characteristics and the shape memory properties. Compared to the original material, the nanocomposite showed an increase of 50% in the elastic modulus (1 wt% of nanocellulose) and a higher maximum tensile stress. At the same time, the creep deformation got lower as the cellulose fraction increased, and no significant change was measured in the recovery rate compared to the one observed for the pure SMP, which is of the order of 95%.

Bin Xu et al. [187] added clay powder as fillers to PU matrix. They investigated the effect of the reinforcement on the behavior and properties of the formed nanocomposite. The mechanical characteristics, such as the elastic modulus and strength, improved while the recovery rate decreased slightly. The storage modulus was also enhanced, but only at room temperature. CNTs have exceptional mechanical and electrical properties, according to multiple studies. [188]. Ly et al.[55] used CNT as fillers to a PU-based SMP matrix to make an FFF filements. The material has a glass transition temperature at 35 °C. The produced parts have an electrical resistance up to 2.27 kOhm. Depending on the layer thickness, the restoring time ranges

between 42 s and 230 s. The studied material is expected to be applied in smart textile. Wan et al.[177] created a direct ink writing (DIW) ink by reinforcing a PLMC matrix with CNT. They produced electrically-responsive parts with different geometries. The electrical conductivity can reach 106 $S.m^{-1}$ with 11.11% CNT weight ratio. Both shape fixity and shape recovery ratios are equal to 100% after 4 cycles. The elastic modulus and tensile strength are up to 1016.8 MPa and 26.2 MPa, respectively. The studied material can be applied to smart electronics.

6. Stimulus responsive materials

The sensitivity of the mechanical properties of shape memory materials to specific stimuli gives them the capacity to change their shape stably and to find their initial shape under the influence of an external stimulus. Several stimuli can be used to activate the shape memory characteristic of a polymer: water [189], heat[123], UV light[190], electricity[191]. Also, pressure-sensitive materials can be used for 4D printing soft pneumatic actuators that change form depending on pressurized or vacuum environment [192].

6.1. Thermo-responsive materials

The property that enables the temperature-responsive shape memory effect comes from a specific molecular structure that can be temporarily changed. Polymers such as starch are often in the form of amorphous solids, i.e., without medium and short-range molecular order, unlike crystalline solids. They are hard and fragile like glass when the temperature is lower than T_g (we speak then of a "glassy state"). When the temperature exceeds T_g, they become rubbery, soft, flexible, and thus have a great capacity for deformation. This glassy to malleable state transition has the advantage of being reversible; for starch, for example, it is expressed at around 120 °C.

The first step is the "programming" of the material, which consists of mechanically deforming it at a temperature higher than the glass transition temperature ($T > T_g$) until the desired secondary shape is obtained. The material is cooled during the second step, while maintaining the applied force. Then, the stress is released, resulting in a slight elastic return of the material.

If no heat treatment is applied, the secondary shape is retained at this stage. Finally, the initial or permanent shape is restored by heating the material, free of external forces. The temperature beyond which the material must be heated to fix the secondary shape and regain the permanent shape is within the glass transition range of the material.

Duan et al.[193] created an SLA-printable thermo-responsive material by mixing thermochromic segments with acrylic resin. After modifying the thermochromic agent by adding γ-methacryloxypropyltrimethoxysilane, the elastic modulus and tensile strength of the new ink were up to 982.24 MPa and 43 MPa, respectively, which consist an increase by 50.77% and 33.83%, respectively, compared with pure acrylic resin. The printed parts changed colours from pink or blue to colourless when the temperature exceeded 31 °C (transition temperature). The characteristics of the thermochromic material can be exploited in manufacturing smart sensors or temperature-sensitive devices

Han et al.[194] analysed the properties of a thermo-responsive poly(N-isopropylacrylamide) (PNIPAAm) hydrogel parts printed via micro-stereolithography (**Figure 9.a**). The printed parts can expand their volume by 186% when the temperature was raised from 10 °C to 50 °C and reversibly regain their original volume when the temperature was set back to 10 °C. It was found that the swelling and shrinking of the parts can be controlled by changing the molar ratios of cross-linker and monomer concentrations, respectively. Higher cross-linker ratio results in shorter polymer chain length and consequently reducing the swelling degree at low temperature (10 °C). In contrast, when increasing the monomer concentration, the swelling ratio increased at high temperature (50 °C). Also, as the layer thickness increases, a disparity of the lateral and vertical swelling of the specimens is observed. This disparity is explained by the fact that the cross-linking density became less uniform as the layer thickness increased. The study showed promising results for future robotics, aerospace, or medical applications.

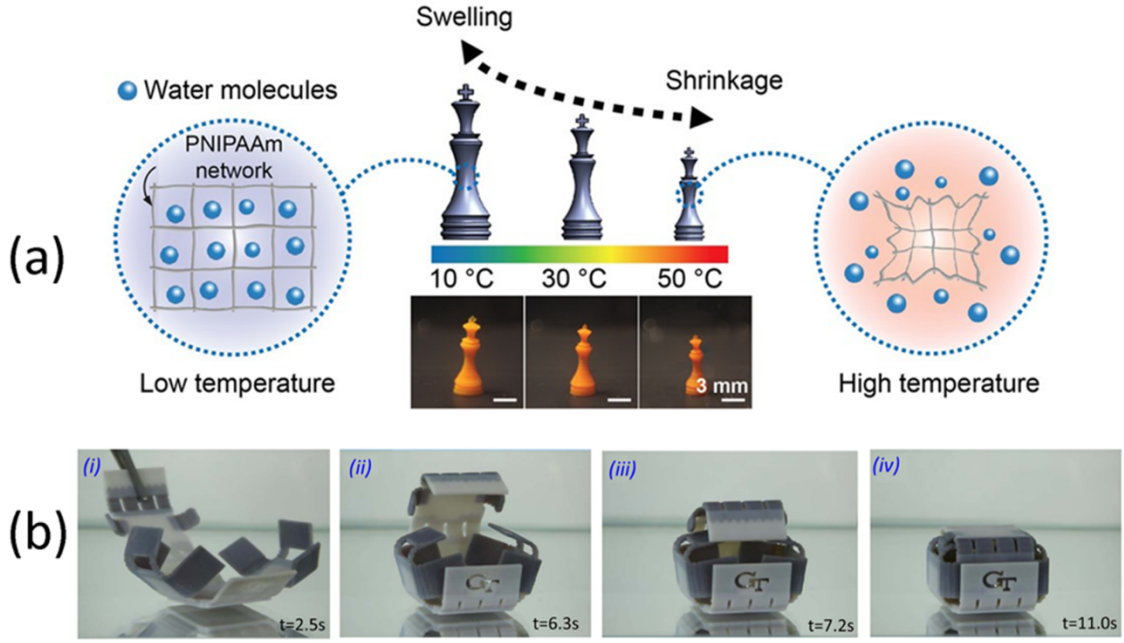

Figure 9. a. Thermally responsive 3D printed shape memory hydrogel structure. Reproduced from. [194]. b. Self-folding thermo-responsive SMP structure. Reproduced from. [195].

Senatov et al.[196] studied the mechanical and shape memory properties of SMC made of PLA matrix reinforced with hydroxyapatite. The shape memory effect of the FFF-printed scaffolds is triggered at 54 °C that corresponds to glass transition temperature of the material. Under compression load, the specimens made from SMC have an elastic modulus and yield strength equal to 2091 MPa and 34.3 MPa, respectively, which consists an increase by 35.3% and 60%, respectively, compared to the specimens made from pure PLA. The shape recovery ratio of the composite parts is up to 98.2% but their structure showed delamination after only 3 cycles. Microscopic observation showed that the material has a "partially" self-healing property. In fact, after heated over its T_g, the cracks within the printed samples are partially repaired. The material is studied as a potential solution for bone defect self-fitting implants.

Mao et al.[195] studied the behavior of self-folding thermos-responsive structures (**Figure 9.b**). The authors used different weight ratios of commercial VeroWhite and Tangoblack SMPs to made seven different materials for 3D printing. Their glass transition temperatures range from 32 °C to 65 °C. The disparity in T_gs allows the control of the folding configuration. The

recovery time can be controlled by varying the recovery temperature. To reproduce the shape memory effect, the programming phase must be repeated each time.

6.2. Electro-responsive materials

The insertion of conductive components such as carbon nanotubes [197] or metallic particles [198] can be used to make electro-responsive SMCs. These fillers increase the material's conductivity, enabling the shape memory effect using heat created via the Joule effect.

Shape memory polymers can react directly to electric current [178, 199]. Electro-responsive polymers change in size or form when triggered by an electric current. They are commonly used as actuators [200, 201] and sensors [202, 203]. Electro-responsive polymers can, typically, endure large deformations [98, 204-206]. Electro-responsive polymers can be used in soft robotics and in developing artificial muscles. They have a reversible change, can be in many different shapes, and are usually divided into two main groups: dielectric [207] and ionic [208].

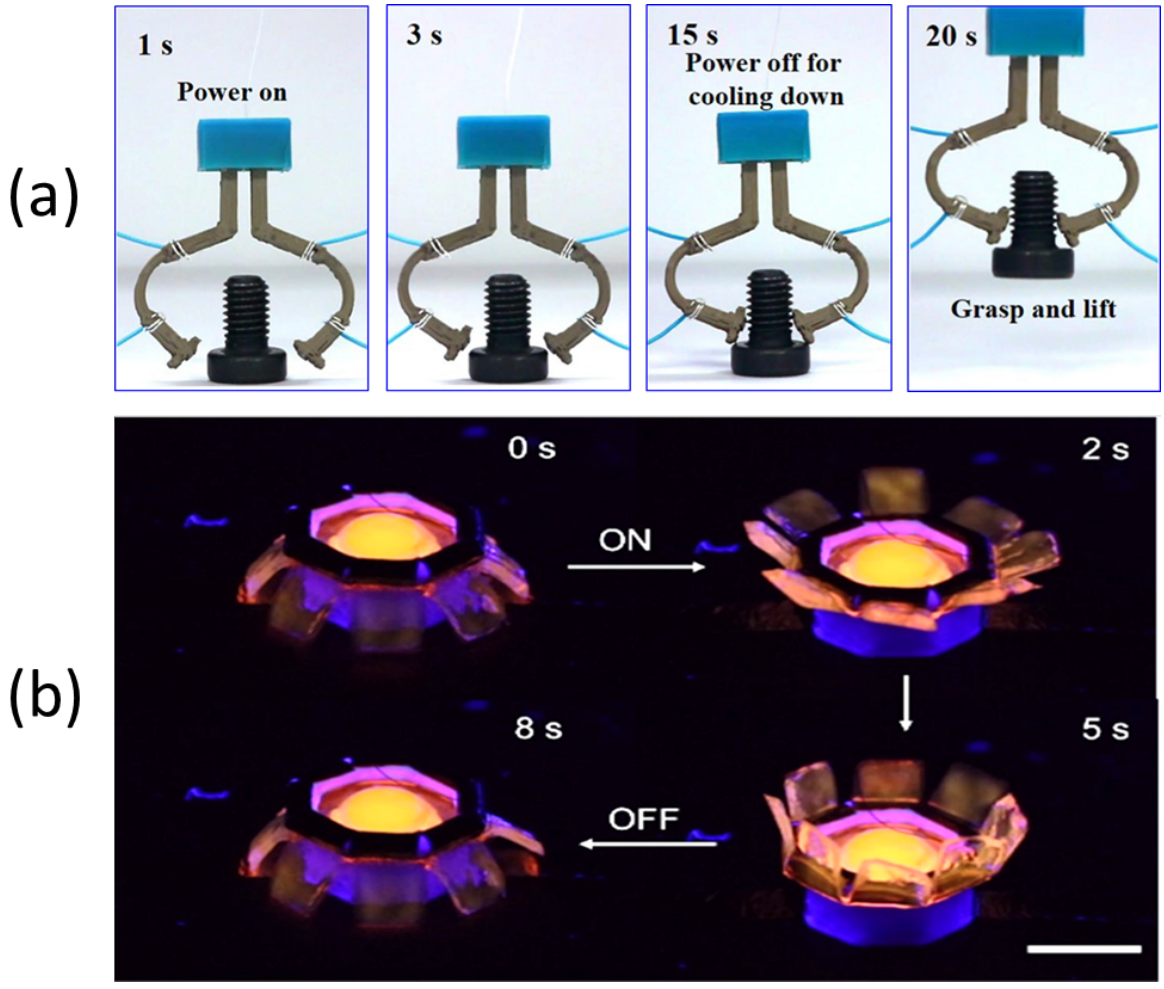

Figure 10. (a) Electro-active grippers made from Ag@CNFs/PLA via direct 3D printing. Reproduced with permission. [176] Copyright 2019, American Chemical Society. (b) 3D printed PVC gel jellyfish actuator under an applied 1kV voltage. Reproduced with permission. [209] Copyright 2021, American Chemical Society.

Figure 10.a represents electro-active grippers made from Ag@CNFs/PLA and printed with 3D process. When subjected to an electric current (1 V), the shape memory effect is activated by the Joule effect and the temperature reaches 80 °C after 15 s. Then the current is turned off to let the grippers cool down and grab an 8 g bolt. **Figure 10.b** shows a 3D printed PVC gel jellyfish actuator that changes shape under an applied 1 kV voltage. The shape memory cycle is reversed within 8 seconds.

6.3. Magnetic-responsive materials

The magnetic field can indirectly enable a shape memory response of a material. By incorporating magnetic particles (generally ferrite and soft magnetic materials) within SMPs, magnetism-driven SMPCs are able to generate heat with Joule effect under a magnetic field and subsequently triggering the shape recovery process [210]. Magnetically sensitive SMCs shrink in a strong magnetic field and thus have applications in drug and cell delivery [179].

Testa et al. [211] have developed a new composite material with magneto-responsive properties. It consists of a silicone-based polymer and droplets of water and glycerine in which iron-carbonyl particles are suspended. These particles provide the magnetic properties of the composite material and its shape memory, which is activated by magnetic fields. Applications for this new composite material include medicine, space travel, electronics, and robotics.

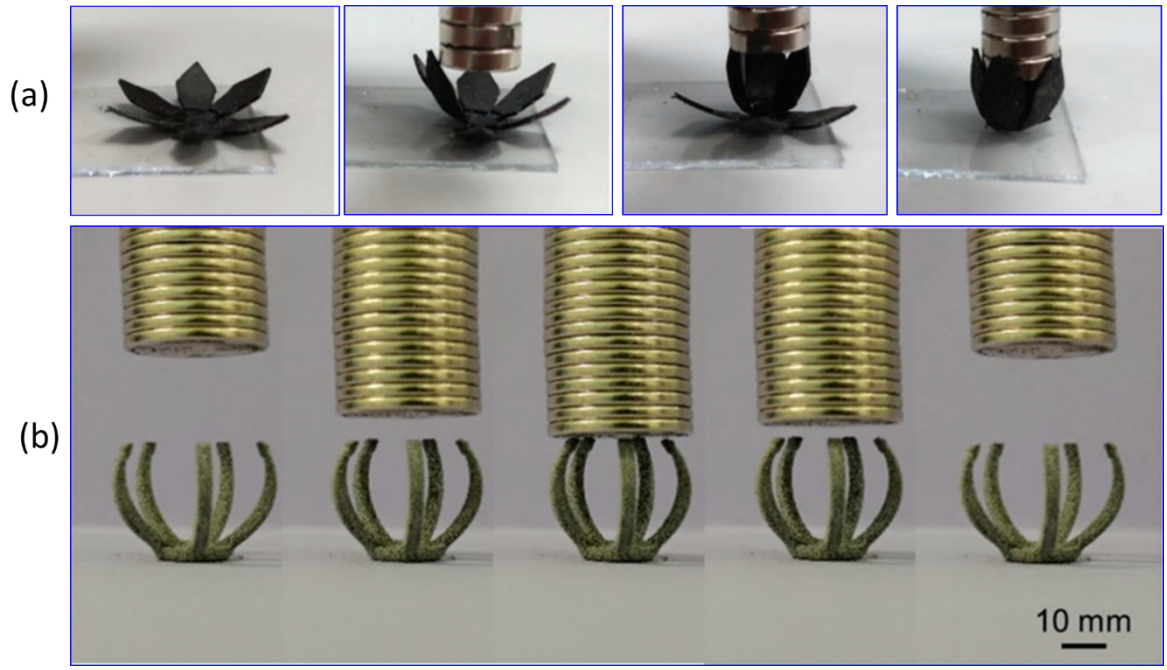

Figure 11. Magnetically responsive parts: (a) 3D printed flower that encloses in the presence of a magnetic field. Reproduced with permission. [212] Copyright 2019, Wiley. (b) Shape memory behavior of a smart gripper under the magnetic stimulus. Reproduced with permission.[213] Copyright 2021, American Chemical Society.

Figure 11.a shows a magneto-responsive flower made from Ebecryl 8232 (Eb), butyl acrylate (BA) and Fe_3O_4 nanoparticles and printed with DLP process. In the presence of a magnetic field the nanocomposite flower encloses. **Figure 11.b** shows an SLS- printed gripper made from TPU matrix and filled with 40 wt % of magnetic Nd2Fe14B powder. In the presence of a magnet, the gripper is closed and it recovers its original shape as soon as the magnetic stimulus is removed.

6.4. Light responsive materials

The concentrated intense light induces stress relaxation to the flex-joints of photo-reactive polymers. These joints are in a stressed state after printing and they deform when exposed to light. The heat generated by the light intensity triggers the shape recovery process. Generally, these light-responsive materials are polymer blends mixed with a photo-initiator, resulting in a

covalently cross-linked amorphous polymer. When light bands stimulate the material with a particular wavelength, the photo-initiator is dissipated. The polymer blend is then polymerized, enabling the stress relaxation of the material [214]. Jin et al.[25] created a single-component robot using a crystalline SMP. The material is a polyurethane-based blend that has thermo- and photo-reversible bonds. To program the 3D-printed parts, the samples were uniaxially loaded at 80 °C under UV-light. The permanent shape was recovered at 140 °C.

Some studies explored the behavior of structures made of light-responsive polymers; Nakano et al. [215] fabricated and studied the behavior of molecular fibers capable of bending when stimulated with laser light. The light polarization direction can control the material's motion direction. Bai et al. [216] made a light-responsive SMC from graphene oxide and thermoset polyurethane. The new material displayed good shape memory behavior (95% shape recovery ratio and self-healing capacity). The composite can also be programmed multiple times without losing its shape memory characteristics, making it adaptable for various applications such as light actuators and self-healing skins.

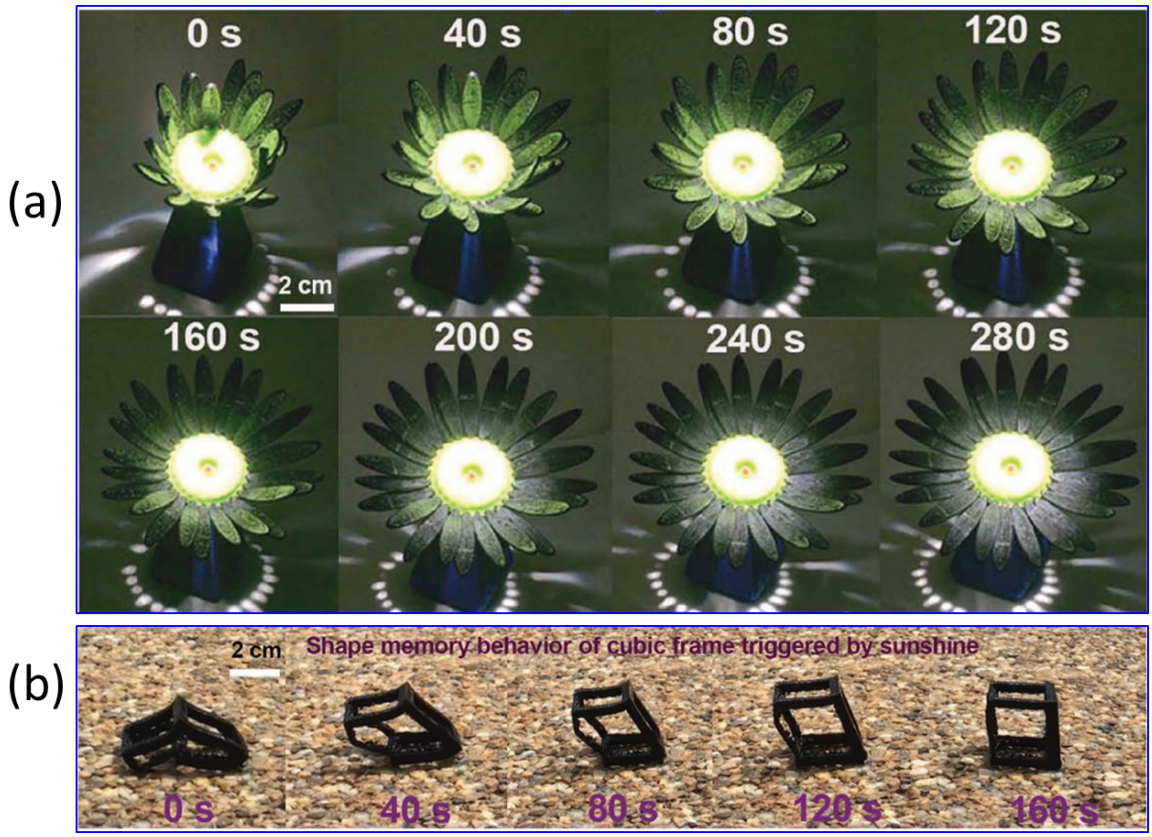

Figure 12. (a) Blooming flower under light exposure. Reproduced with permission. [62] Copyright 2017, Wiley. (b) Cubic structure shape memory behavior under sunshine exposure. Reproduced with permission. [62] Copyright 2017, Wiley.

Figure 12.a shows an FFF printed sunflower made from PU/CB SMC. The sunflower is exposed to light with an intensity of 87 m.W.cm^{-2}. It recovers its original full blooming shape within 280 s. **Figure 12.b** represents a cubic structure made from the same material and printed with the same technique. Sunlight with an intensity of 76 m.W.cm^{-2} enables the cubic part to switch from its temporary shape to its permanent one in just 160 s.

6.5. pH-responsive materials

Hu et al. [217] created micro-size elements with a hydrogel that change form in response to pH level variations. The specimens were inspired by plants and flowers' behavior. They were printed using the direct ink printing technique. The time response is less than half a millisecond. This property, along with the microscale size, and the pH-responsive behavior, make this material a good candidate for biomedical application. Dutta et al.[218] made a shape-memory

hydrogel by mixing methacrylated polyethylene oxide, polypropylene oxide, and polyethylene oxide. They used it to produce pH-sensitive parts via the SLA process. The 3D printed structures showed more expansion (up to 40 times) at higher pH levels (7.4). These structures can potentially be applied in medical devices production.

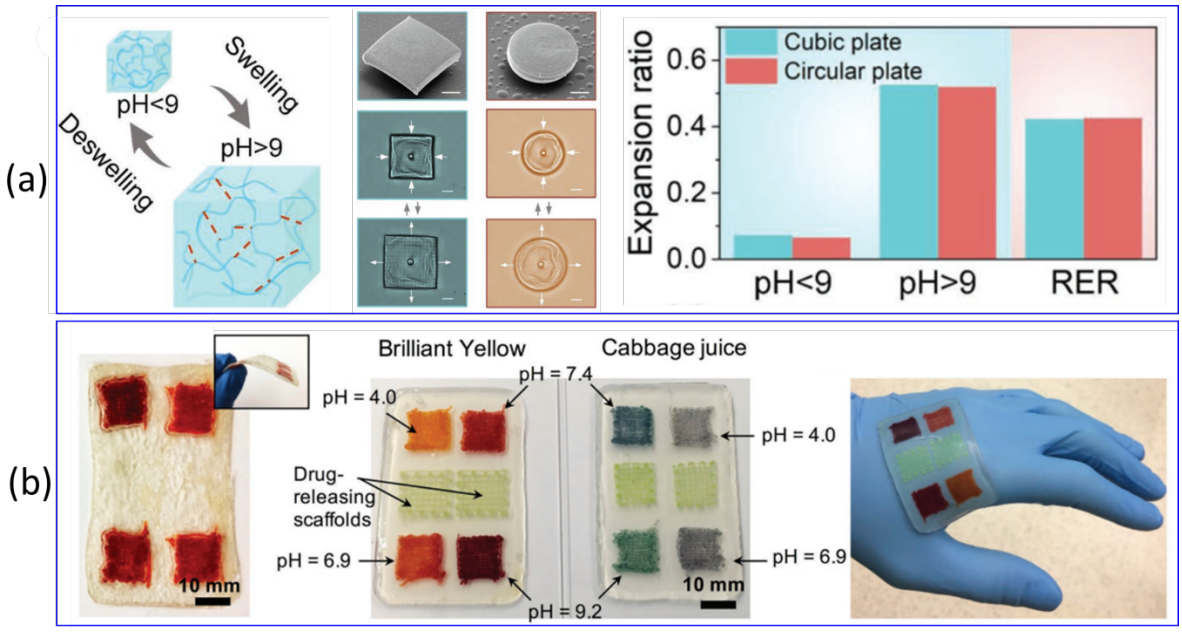

Figure 13. (a) 3D printed SMP micro-parts structures and their response to pH variation. Reproduced with permission. [217] Copyright 2020, Wiley. (b) pH-responsive multi-functional wound dressing. Reproduced with permission. [219] Copyright 2017, Wiley.

Nadgorny et al. [220] studied the behavior and the thermomechanical properties of a synthesized pH-responsive hydrogel. The combination of poly(2-vinylpyridine) (P2VP) with ABS made the printable material give the samples better mechanical characteristics. The 3D process used is the 3DP. The printed samples showed two-way swelling behavior.

Figure 13 presents pH-responsive 3D printed parts. **Figure 13.a** represents shape memory hydrogel microparts, printed with DIW process. When immersed in a NaOH solution with a pH level superior to 9, the parts exhibit an immediate swelling behavior. After adding HCl solution, the pH level decrease under 9 and the microparts contracted. The expansion ratios are 53% and 52% for the cubic and circular parts, respectively. And the contraction ratios are 7.2% and 6.6% for the cubic and circular parts, respectively. **Figure 13.b** shows a multi-functional wound

dressing that can measure the pH level in the wound using an array of pH-responsive sensors and therefore assess the degree of bacterial infection. Then, antibiotics are released to sterilize and heal the injury. The wound dressing is used as a patch capable of maintaining contact with the skin surface.

6.6. Moisture responsive materials

Hydrogels are macromolecular polymer gels. Their hydrophilic polymer chains can be physically or chemically linked together. Hydrogels may significantly expand by absorbing water molecules in their network structure. As a result, hydrogels volume can change dynamically in response to changes in ambient humidity. This property can be exploited used in expandable, folding, or bending smart structures [221]. Zhang et al. [222] studied a cellulose-based material able to react to moisture. They developed a two-layer film using cellulose and steroid esters with different degrees of substitution on each side. The first one is very hydrophilic, while the second one is very hydrophobic. When the samples' temperature decreased from 50 °C to 22 °C, the relative humidity increased from 5.9% to 35 °C. At 22%, the hydrophobic facet contracted and the hydrophilic one expanded causing the twisting of the sample. The samples' behavior is reversed when inverting the temperature and humidity conditions.

Baker et al. [223] studied the properties of multi-material moisture-responsive origami structures as shown in **Figure 14.a**. The FFF-printed parts are three-layered as a sandwich structure. The core of the structure is made from hydrophilic polyurethane hydrogel and it acts as the active component. It is wrapped in between two layers of hydrophobic polyurethane elastomer which constitute the passive component. The glass transition temperatures of the used hydrogel and elastomer are -47 °C and -35 °C, respectively. The folding process is activated by hydrating the samples. The layers' thickness and length are used to control the range and speed of the shape memory effect.

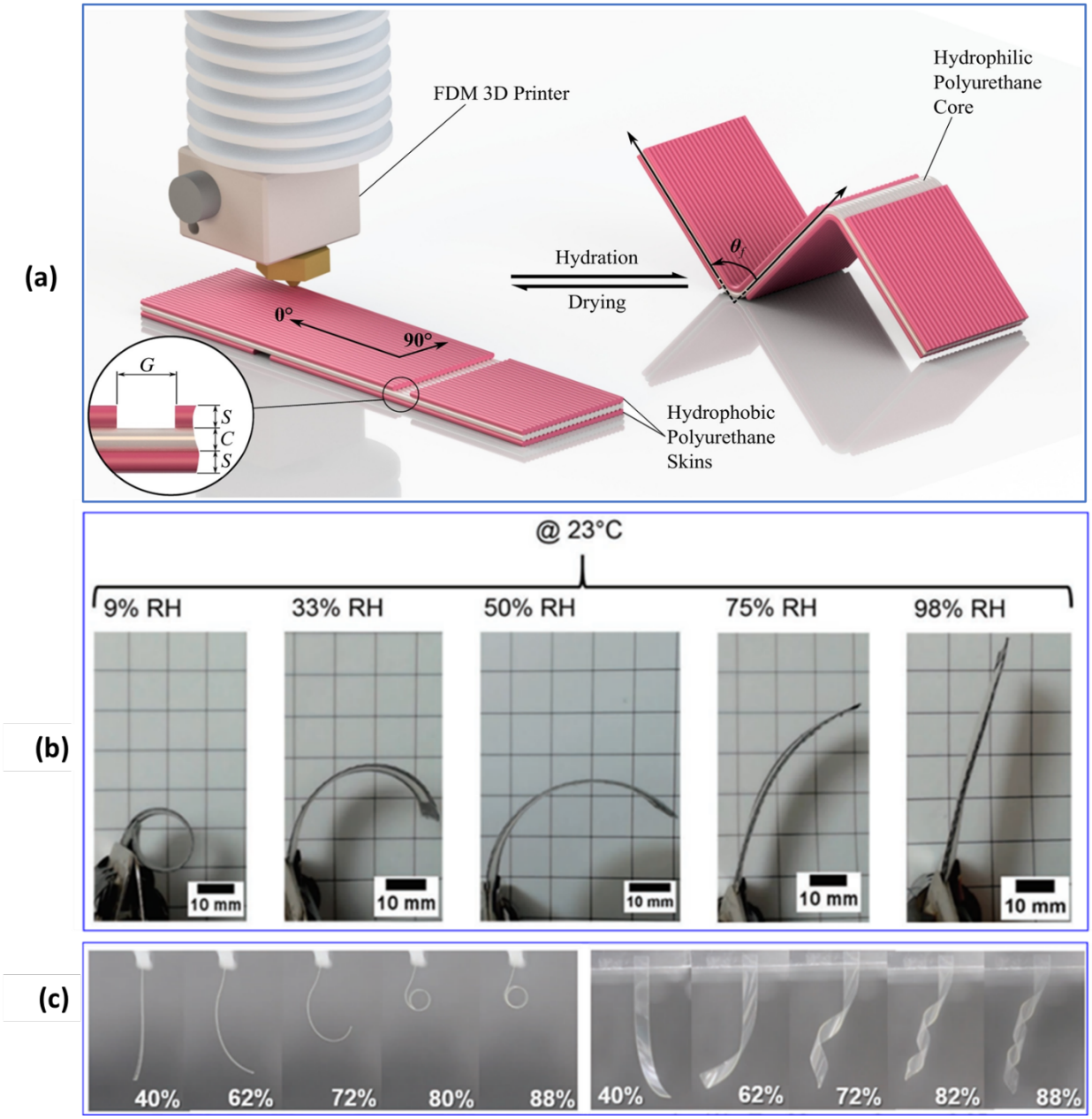

Figure 14. a. 3D-printing of self-folding multi-materials moisture-responsive structure [223]. Copyright 2019, Elsevier. b. Shape evolution of 3D printed sample made from Polyamide and carbon fibers with humidity increase [22]. Reproduced with permission. Copyright 2019, Wiley. c. Shape evolution of liquid crystal elastomer parts under different humidity conditions. Reproduced with permission. [224] Copyright, Wiley.

Siqueira et al. [225] created a SMC made from a mixture of 2-hydroxyethyl methacrylate (HEMA) and polyether urethane acrylate (PUA) as the matrix and reinforced with cellulose nanocrystals (CNC). The material is used as ink for DIW process. The effect of CNC fillers on

the mechanical properties of the printed parts was evaluated. By adding 10 wt% and 20 wt% of CNC to 1:1 weight ratio of HEMA and PUA, the elastic modulus of the material is enhanced by 32% and 80%, respectively. Samples with 10 wt% of CNC have higher tensile strength in the longitudinal and transverse by 34% and 13%, respectively.

Correa et al. [226] investigated the properties of a SMC consisting of ABS or nylon-based polymers reinforced with wood filaments. The FFF-printed parts are moisture-responsive. The shape memory effect is triggered by water submersion. The shape transformation is reversible with air or heat drying and can undergo up to 30 cycles (for the case of ABS/wood SMC) without any significant damage or degradation. In the case of nylon/wood SMC, increasing the thickness of nylon creates faster response and wider range of shape morphing. The integration of SMPs decreases the humidity absorption by the wood fillers slowing down its expansion but enhances the overall material's elasticity and durability.

The deformation pattern results from the structuring of the material layers and the grain of the wood composite layers. It provides faster and greater deformation. Both methods allow the materials to deform reversibly when exposed to humidity.

Figure 14.b shows an SMC part made from a polyamide matrix and carbon fibers fillers. The sample recovers its straight shape when humidity increases from 9% to 98% at a constant temperature of 23 °C. **Figure 14.c** shows humidity-responsive parts made from liquid crystal elastomer. The humidity level increase from 40% to 88% enables the samples transform from straight to folded and twisted shapes.

7. Advanced Applications and perspectives of 4D printing

4D printing is very promising in fields such as biomedical applications [227], aerospace [26], military [228] and automotive industries [229].

Gladman et al. [230] are investigating the possibility of using 4D printing to create bio-inspired structures, which exploit the shape changes of a hydrogel in the presence of a chemical stimulus

such as water. Objects printed in this material can transform to adopt architecture reminiscent of those seen in flowers. In nature, the composition and microstructure of tissues change depending on the plant's environment. In order to reproduce this process, the researchers designed a composite based on a 4D printed hydrogel mixed with cellulose fibers to control water absorption. The printed flower changes shape when it comes into contact with water, in the same way a plant reacts to humidity, temperature change, or any other environmental stimulus.

Han et al. [194] developed hydrogels sensitive to physical stimuli, such as temperature. Their micro-stereolithography technique allows 3D printing of objects from gels whose shape changes with temperature. This type of 4D structure could lead to the construction of shock absorbers for deformable robots or medicines delivered directly to their targets.

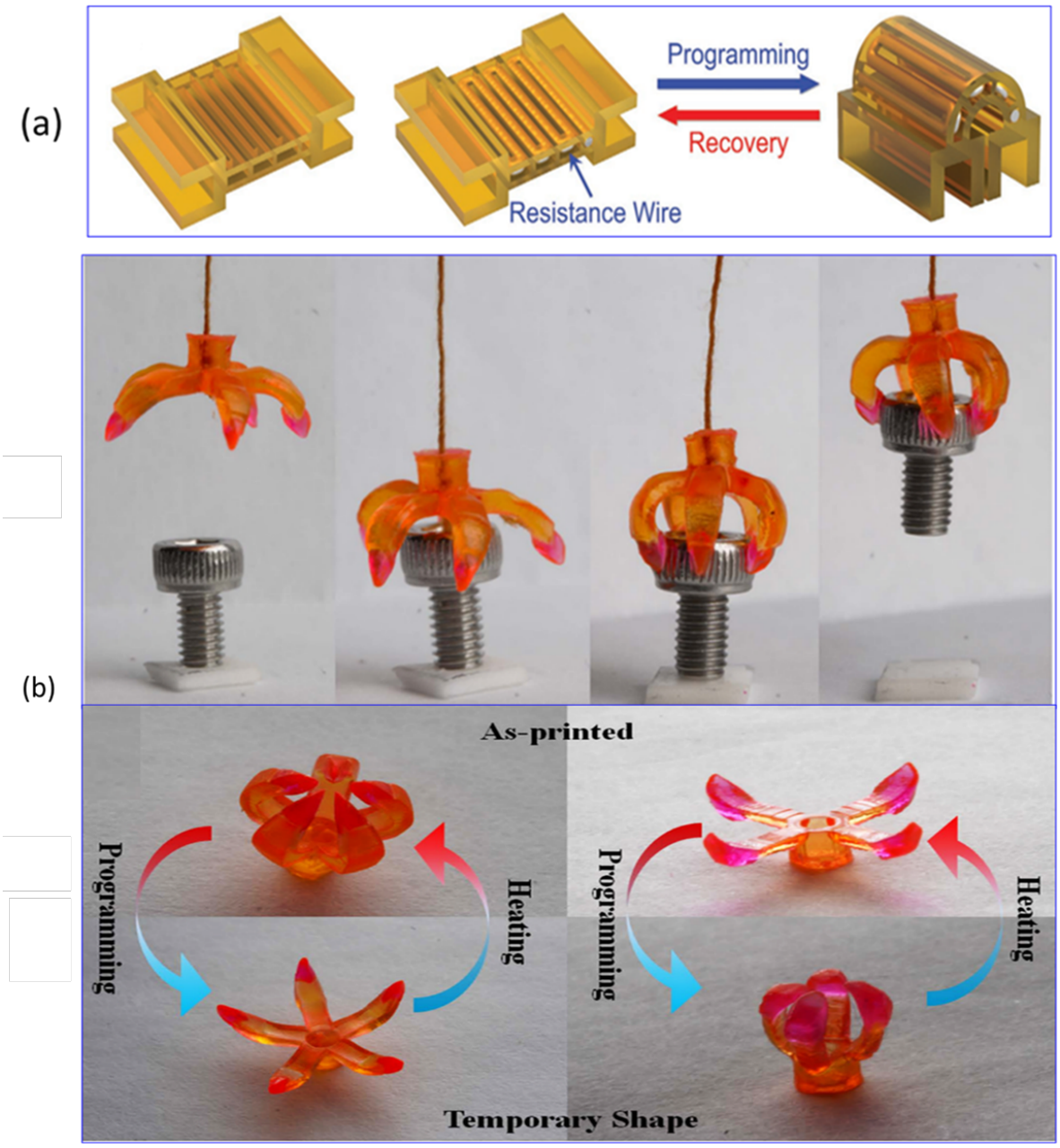

Figure 15. (a) DLP printed SMP smart hinge. Reproduced with permission. [86] Copyright 2021, Wiley. (b) 3D printed shape morphing grippers. Reproduced from. [117].

Chen et Shea [231], have fabricated multi-material objects using a Stratasys Objet3 Connex500 printer based on two shape-memory polymers, a rigid heat-resistant polymer and an elastomer-like polymer. Printed in 2D, these objects expand to form a 3D load-bearing structure when immersed in hot water. The ability to change their load-bearing capabilities over time is of particular interest to space exploration, architecture, construction, and the automotive industry.

Zhang et al. [86] designed a multi-material smart hinge made from an SMP consisting of *t*BA and AUD with microchannels filled with resistance metallic wire as shown in **Figure 15.a**. The soft parts are produced with the DLP process. When an electric current o 3.7 A is passed through those wires, they are heated to 80 °C by the Joule effect, which activates the smart hinge's shape recovery. Ge et al.[117] designed shape memory grippers made from BMA/PEGDMA/BPA/DEGDMA (**Figure 15.b**). The micro-stereolithography grippers are thermally-sensitive. They exhibited a 330% maximum strain at 40 °C and had 90% and 95% shape fixity and shape recovery ratios, respectively. The glass transition temperature ranges between 50 °C and 180 °C, depending on the ink components' weight fraction.

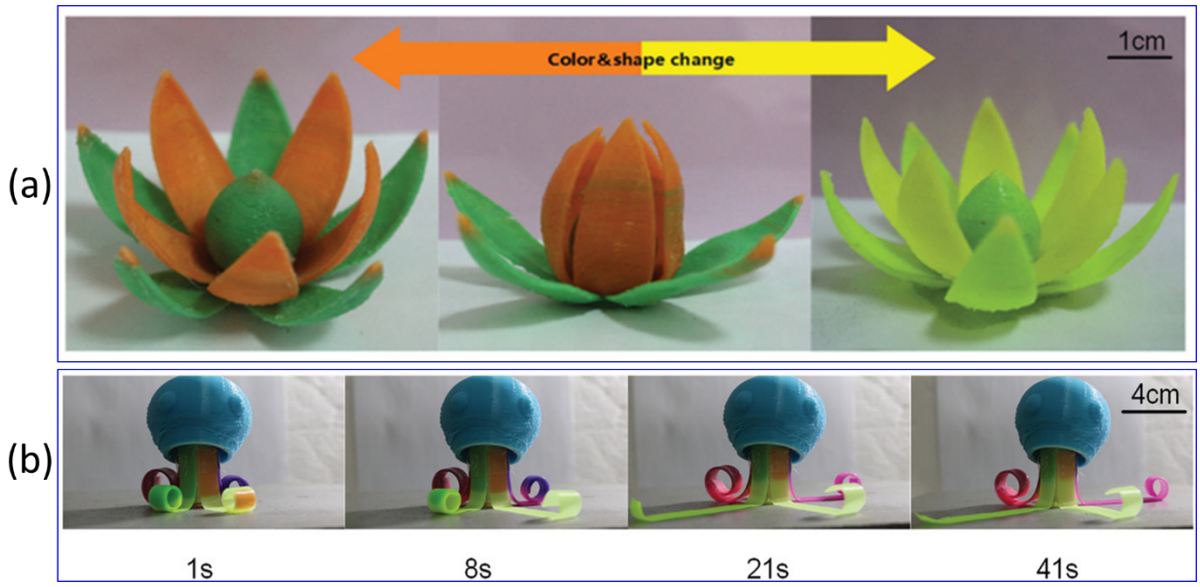

Figure 16 Colour changing 4D-printed parts (a) FFF-printed shape and colour shifting flower. Reproduced with permission [232] Copyright 2019, Wiley. (b) FFF-printed shape morphing octopus. Reproduced with permission. [232] Copyright 2019, Wiley.

4D printing can also be used in aesthetic applications. **Figure 16.a** shows the shape morphing and colour shifting of FFF-printed specimens. The printed parts are made from PLA, thermochromic powder, stearic acid amide, and polyethylene wax. As the printed flower change shape from enclosing to blooming, the petals change colour from green and orange to fluorescent green. **Figure 16.b** shows the shape memory morphing and of an FFF-printed

octopus. The tentacles changed colour and form from curled to stretched when exposed to 80 °C temperature. Each tentacle was produced with different printing parameters to control their recovery chronologically. For instance, higher nozzle temperature and height lead to faster shape recovery. Inversely the increase in layer thickness slows down the shape recovery.

Miao et al. [233] made a photocurable SLA-printable resin that comprises a renewable, soybean oil-based, biocompatible epoxy acrylate. The printed samples are biocompatible. They recovered 100% of their original shape when the temperature varied between -18 °C to 37 °C. The scaffolds printed with the studied resin enabled human bone stem cells to grow. Scientists think this material will be a big help in developing biomedical scaffolds because it has a strong shape memory effect and is safe for people to use.

Apsite et al. [234] have developed a new approach to print biocompatible and biodegradable morphology-modified hydrogels. Self-replicated hollow tubes can be manufactured. Their diameters can be controlled at high resolution (20 μm), simulating blood vessels. The process was applied on two different polymers; alginate and hyaluronic acid and mouse bone marrow stromal cells. The proposed 4D process does not affect the viability of the printed cells, which was maintained for a week at least. Therefore, this advanced 4D printing technique is a promising advancement in the biomedical field.

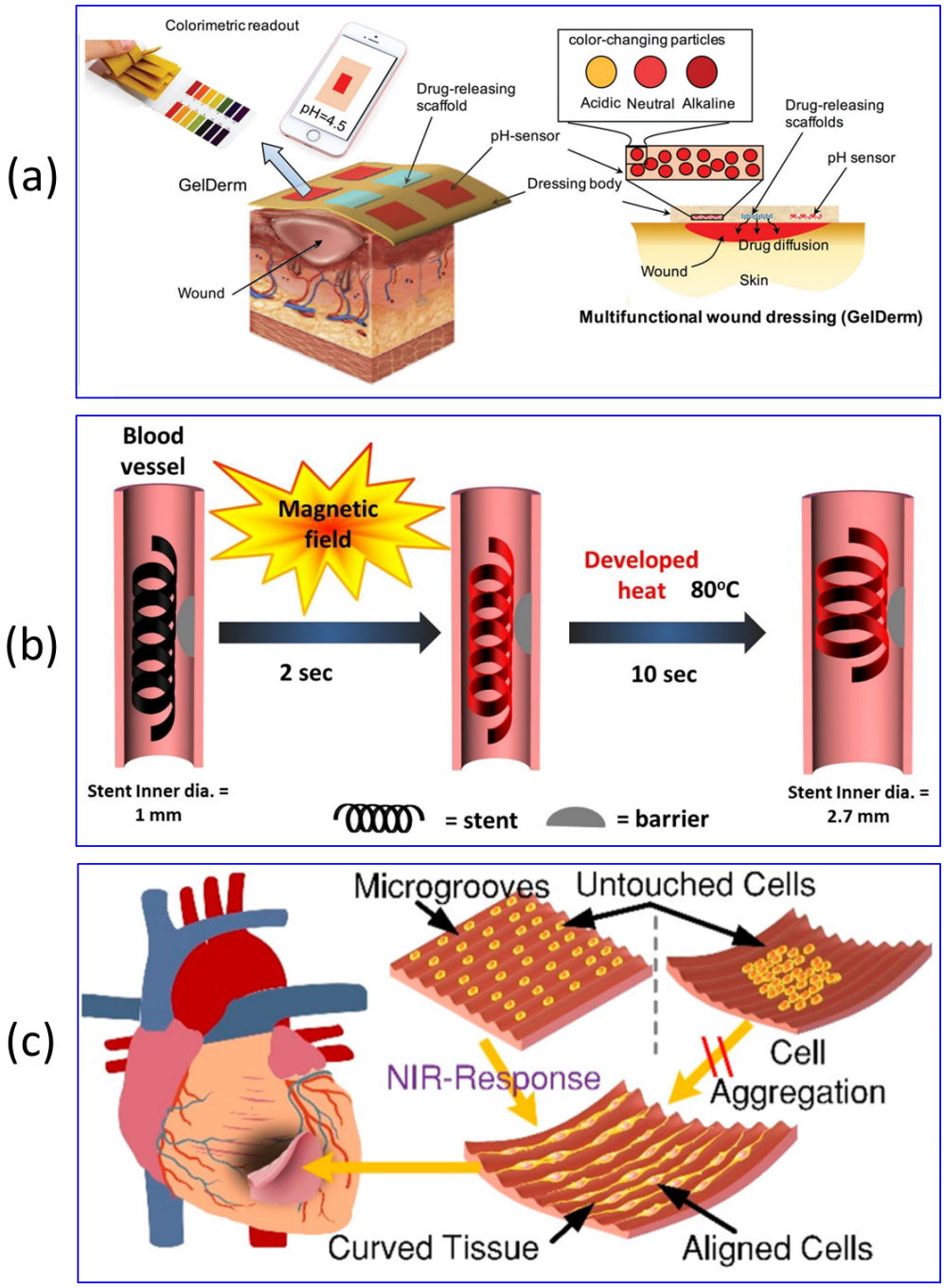

Figure 17 Advanced medical application for 4D printing: (a) Multifunctional pH-responsive wound dressing. Reproduced with permission. [219] Copyright 2017, Wiley. (b) Intravascular stent scaffold. Reproduced with permission. [235] Copyright 2019, American Chemical Society. (c) DLP printed cardiac patch that mimics myocardial tissue. Reproduced with permission. [236] Copyright 2021, American Chemical Society.

Figure 17.a is a schematic illustration of a multifunctional pH-sensitive wound dressing. The smart dressing can assess the degree of the injury infection by detecting the pH level in the epidermal wounds (A healthy skin pH level is between 4 and 6 while an injured one is 7.4 [237]). And accordingly, the multifunction dressing release a sterilizing and healing drug. **Figure 17.b** is a schematic illustration of a DIW-printed intravascular stent made from c-PLA/Fe_3O_4 composite. The stent has five layers with 500 μm interfilament space. The printed part can expand to facilitate the blood flow in the blood vessel by an alternating magnetic field with a 30 kHz frequency. This process is achieved within 10 s. **Figure 17.c** illustrates a 4D printed cardiac patch that can enable myocardial tissue repair after myocardial infarction. The patch is DLP-printed and made from PEGDA based hydrogel filled with 15% graphene. The ink is light-sensitive and has a glass transition temperature of around 45°C.

8. Conclusion and perspectives

In this paper, the different aspects of 3D printing were discussed: the fundamentals of the most conventional processes, the types of materials used in each one, as well as their advantages and limits. Each process is characterised by the layering mechanism it uses, the form of the required material (filament for FFF and liquid for SLA, for example), and the properties of the produced parts (resolution, mechanical properties...). The shape memory polymers that upgrade basic additive manufacturing to 4D printing were then investigated: the mechanisms that accord them their shape memory properties, the blends and composites that can be derived from them, and the different stimuli that activate the shape memory function.

4D printing is emerging as a promising technology in many fields. It has been successfully used to solve problems that were so far impossible (or extremely costly) to solve with conventional manufacturing techniques. The smart material, particularly shape-memory polymers and their derivatives (blends and composites), is the key factor in this technology. Their reactivity to their

environment gives them a valuable potential for customized and atypical applications like medicine delivery systems and microfluidics.

Due to their unique microstructure, SMPs can change form over time. A shape memory polymer essentially has two microphases: soft and hard segments. The first one gives the material an elastic behavior, while the second one strengthens the material. The transition from one behavior to another is activated by an external stimulus (heat, electrical current, light, etc.).

A wide range of shape memory polymers, blends, and composites have been developed and tested as possible inks for 4D processes. The main challenges are related to the compatibility of the inks' components (polymer/polymer for polymeric blends and matrix/reinforcements for composites) and to the compatibility of the developed material with the 3D printing technique. Reinforcing shape memory polymers can add to the material's properties and functionalities. However, it considerably affects the "printability" of the material, leading to important compromises. Furthermore, most of the commonly used shape-memory materials in 4D printing can only provide basic shape memory functions. SMPs cannot change shape repeatedly without losing their mechanical and shape memory properties over time.

In addition, a major disadvantage is the volume limitation of 3D printing systems. The printed parts cannot be made in extensive amounts or large sizes, yet.

4D printing will continue to evolve as many aspects of the technology are currently under investigation: manufacturing techniques, smart printable materials, geometry design (auxetic and origami structures), simulation and modelling tools, and 3D printing of larger volumes [238]. Printing multi-material or multi-stimuli responsive parts also paves the way for new and challenging opportunities in 4D printing.

References

1. Gebhardt, A., *Understanding Additive Manufacturing*, in *Understanding Additive Manufacturing*, A. Gebhardt, Editor. 2011, Hanser. p. I-IX.
2. Pagac, M., et al., *A Review of Vat Photopolymerization Technology: Materials, Applications, Challenges, and Future Trends of 3D Printing.* Polymers, 2021. **13**(4): p. 598.
3. Gibson, I., et al., *Additive Manufacturing Technologies*. 2020.
4. Liu, G., et al., *Additive manufacturing of structural materials.* Materials Science and Engineering: R: Reports, 2021: p. 100596.
5. Lee, J.-Y., J. An, and C.K. Chua, *Fundamentals and applications of 3D printing for novel materials.* Applied materials today, 2017. **7**: p. 120-133.
6. Bai, Y. and C.B. Williams, *An exploration of binder jetting of copper.* Rapid Prototyping Journal, 2015. **21**(2): p. 177-185.
7. Martin, J.H., et al., *3D printing of high-strength aluminium alloys.* Nature, 2017. **549**(7672): p. 365-369.
8. Stansbury, J.W. and M.J. Idacavage, *3D printing with polymers: Challenges among expanding options and opportunities.* Dental materials, 2016. **32**(1): p. 54-64.
9. Hwa, L.C., et al., *Recent advances in 3D printing of porous ceramics: A review.* Current Opinion in Solid State and Materials Science, 2017. **21**(6): p. 323-347.
10. De Schutter, G., et al., *Vision of 3D printing with concrete—Technical, economic and environmental potentials.* Cement and Concrete Research, 2018. **112**: p. 25-36.
11. Shirole, A., et al., *Shape memory composites based on electrospun poly (vinyl alcohol) fibers and a thermoplastic polyether block amide elastomer.* ACS applied materials & interfaces, 2016. **8**(10): p. 6701-6708.
12. Bikas, H., P. Stavropoulos, and G. Chryssolouris, *Additive manufacturing methods and modelling approaches: a critical review.* The International Journal of Advanced Manufacturing Technology, 2016. **83**(1): p. 389-405.
13. Siemasz, R., K. Tomczuk, and Z. Malecha, *3D printed robotic arm with elements of artificial intelligence.* Procedia Computer Science, 2020. **176**: p. 3741-3750.
14. Placone, J.K. and A.J. Engler, *Recent Advances in Extrusion-Based 3D Printing for Biomedical Applications.* Advanced Healthcare Materials, 2018. **7**(8): p. 1701161.
15. Kumar, L.J. and C.G. Krishnadas Nair, *Current Trends of Additive Manufacturing in the Aerospace Industry*, in *Advances in 3D Printing & Additive Manufacturing Technologies*, D.I. Wimpenny, P.M. Pandey, and L.J. Kumar, Editors. 2017, Springer Singapore: Singapore. p. 39-54.
16. Lee, A.Y., et al., *Contactless reversible 4D-printing for 3D-to-3D shape morphing.* Virtual and Physical Prototyping, 2020. **15**(4): p. 481-495.
17. Andre, J. *From Additive Manufacturing to 3D/4D Printing 3: Breakthrough Innovations: Programmable Material, 4D Printing and Bio-printing*. 2018.
18. Zhou, L.-y., et al., *4D Printing of High-Performance Thermal-Responsive Liquid Metal Elastomers Driven by Embedded Microliquid Chambers.* ACS Applied Materials & Interfaces, 2020. **12**(10): p. 12068-12074.
19. Nishiguchi, A., et al., *4D Printing of a Light-Driven Soft Actuator with Programmed Printing Density.* ACS Applied Materials & Interfaces, 2020. **12**(10): p. 12176-12185.
20. Mulakkal, M.C., et al., *Responsive cellulose-hydrogel composite ink for 4D printing.* Materials & Design, 2018. **160**: p. 108-118.
21. Tibbits, S., *4D Printing: Multi-Material Shape Change.* Architectural Design, 2014. **84**(1): p. 116-121.
22. Le Duigou, A., et al., *Bioinspired Electro-Thermo-Hygro Reversible Shape-Changing Materials by 4D Printing.* Advanced Functional Materials, 2019. **29**(40): p. 1903280.

23. Zhou, Y., et al., *From 3D to 4D printing: approaches and typical applications.* Journal of Mechanical Science and Technology, 2015. **29**(10): p. 4281-4288.
24. Kuang, X., et al., *3D Printing of Highly Stretchable, Shape-Memory, and Self-Healing Elastomer toward Novel 4D Printing.* ACS Applied Materials & Interfaces, 2018. **10**(8): p. 7381-7388.
25. Jin, B., et al., *Programming a crystalline shape memory polymer network with thermo- and photo-reversible bonds toward a single-component soft robot.* Science Advances, 2018. **4**(1): p. eaao3865.
26. Ntouanoglou, K., P. Stavropoulos, and D. Mourtzis, *4D Printing Prospects for the Aerospace Industry: a critical review.* Procedia Manufacturing, 2018. **18**: p. 120-129.
27. Gao, B., et al., *4D Bioprinting for Biomedical Applications.* Trends in Biotechnology, 2016. **34**(9): p. 746-756.
28. Wu, X.L., et al., *Characterization of polymeric shape memory materials.* Journal of Polymer Engineering, 2017. **37**(1): p. 1-20.
29. Champeau, M., et al., *4D Printing of Hydrogels: A Review.* Advanced Functional Materials, 2020. **30**(31): p. 1910606.
30. Monzón, M.D., et al., *4D printing: processability and measurement of recovery force in shape memory polymers.* The International Journal of Advanced Manufacturing Technology, 2017. **89**(5): p. 1827-1836.
31. Caputo, M.P., et al., *4D printing of net shape parts made from Ni-Mn-Ga magnetic shape-memory alloys.* Additive Manufacturing, 2018. **21**: p. 579-588.
32. Santo, L., et al., *Shape memory composites for self-deployable structures in aerospace applications.* Procedia Engineering, 2014. **88**: p. 42-47.
33. Kuang, X., et al., *Advances in 4D Printing: Materials and Applications.* Advanced Functional Materials, 2019. **29**(2): p. 1805290.
34. Hann, S.Y., et al., *4D printing soft robotics for biomedical applications.* Additive Manufacturing, 2020. **36**: p. 101567.
35. Pinho, A.C., C.S. Buga, and A.P. Piedade, *The chemistry behind 4D printing.* Applied Materials Today, 2020. **19**: p. 100611.
36. Lee, J., et al., *A review on 3D printed smart devices for 4D printing.* International Journal of Precision Engineering and Manufacturing-Green Technology, 2017. **4**(3): p. 373-383.
37. Matta, A., et al., *Metal Prototyping the future of Automobile Industry: A review.* Materials Today: Proceedings, 2018. **5**(9): p. 17597-17601.
38. Biswas, M.C., et al., *4D Printing of Shape Memory Materials for Textiles: Mechanism, Mathematical Modeling, and Challenges.* Advanced Functional Materials, 2021. **31**(19): p. 2100257.
39. Quirk, R.P., D.J. Kinning, and L.J. Fetters, *1 - Block Copolymers*, in *Comprehensive Polymer Science and Supplements*, G. Allen and J.C. Bevington, Editors. 1989, Pergamon: Amsterdam. p. 1-26.
40. Rodríguez-Hernández, J., *6 - Micro-/nanostructured polymer blends containing block copolymers*, in *Recent Developments in Polymer Macro, Micro and Nano Blends*, P.M. Visakh, G. Markovic, and D. Pasquini, Editors. 2017, Woodhead Publishing. p. 131-161.
41. Lendlein, A. and S. Kelch, *Shape-Memory Polymers.* Angewandte Chemie International Edition, 2002. **41**(12): p. 2034-2057.
42. Parameswaranpillai, J., et al., *Shape memory polymers, blends and composites*. 2020: Springer.
43. Behl, M. and A. Lendlein, *Shape-memory polymers.* Materials Today, 2007. **10**(4): p. 20-28.

44. Daminabo, S.C., et al., *Fused deposition modeling-based additive manufacturing (3D printing): techniques for polymer material systems.* Materials Today Chemistry, 2020. **16**: p. 100248.
45. Rahim, T.N.A.T., A.M. Abdullah, and H. Md Akil, *Recent developments in fused deposition modeling-based 3D printing of polymers and their composites.* Polymer Reviews, 2019. **59**(4): p. 589-624.
46. Huang, J., Q. Qin, and J. Wang, *A Review of Stereolithography: Processes and Systems.* Processes, 2020. **8**(9): p. 1138.
47. Bártolo, P.J., *Stereolithography: materials, processes and applications*. 2011: Springer Science & Business Media.
48. Zhao, Z., X. Tian, and X. Song, *Engineering materials with light: recent progress in digital light processing based 3D printing.* Journal of Materials Chemistry C, 2020. **8**(40): p. 13896-13917.
49. Zhu, G., et al., *Reprintable Polymers for Digital Light Processing 3D Printing.* Advanced Functional Materials, 2021. **31**(9): p. 2007173.
50. Saadi, M.A.S.R., et al., *Direct Ink Writing: A 3D Printing Technology for Diverse Materials.* Advanced Materials, 2022. **34**(28): p. 2108855.
51. Fellin, C.R. and A. Nelson, *Direct-Ink Write 3D Printing Multistimuli-Responsive Hydrogels and Post-Functionalization Via Disulfide Exchange.* ACS Applied Polymer Materials, 2022. **4**(5): p. 3054-3061.
52. Anelli, S., et al., *Hybrid-3D printing of symmetric solid oxide cells by inkjet printing and robocasting.* Additive Manufacturing, 2022. **51**: p. 102636.
53. Kriegseis, S., et al., *3D printing of complex ceramic dental implant abutments by using Direct Inkjet Printing.* Materials Letters, 2022. **313**: p. 131789.
54. Hu, G.F., et al., *Increasing dimension of structures by 4D printing shape memory polymers via fused deposition modeling.* Smart Materials and Structures, 2017. **26**(12): p. 125023.
55. Ly, S.T. and J.Y. Kim, *4D printing–fused deposition modeling printing with thermal-responsive shape memory polymers.* International Journal of Precision Engineering and Manufacturing-Green Technology, 2017. **4**(3): p. 267-272.
56. Chu, H., et al., *4D Printing: A Review on Recent Progresses.* Micromachines, 2020. **11**(9): p. 796.
57. Lamm, M.E., et al., *Material Extrusion Additive Manufacturing of Wood and Lignocellulosic Filled Composites.* Polymers, 2020. **12**(9): p. 2115.
58. Yang, F., M. Zhang, and B. Bhandari, *Recent development in 3D food printing.* Critical Reviews in Food Science and Nutrition, 2017. **57**(14): p. 3145-3153.
59. Barletta, M., A. Gisario, and M. Mehrpouya, *4D printing of shape memory polylactic acid (PLA) components: Investigating the role of the operational parameters in fused deposition modelling (FDM).* Journal of Manufacturing Processes, 2021. **61**: p. 473-480.
60. Ginoux, G., I. Vroman, and S. Alix, *Influence of fused filament fabrication parameters on tensile properties of polylactide/layered silicate nanocomposite using response surface methodology.* Journal of Applied Polymer Science, 2021. **138**(14): p. 50174.
61. Bakrani Balani, S., et al., *Influence of printing parameters on the stability of deposited beads in fused filament fabrication of poly(lactic) acid.* Additive Manufacturing, 2019. **25**: p. 112-121.
62. Yang, H., et al., *3D printed photoresponsive devices based on shape memory composites.* Advanced Materials, 2017. **29**(33): p. 1701627.
63. Chen, Q., et al., *4D Printing via an Unconventional Fused Deposition Modeling Route to High-Performance Thermosets.* ACS Applied Materials & Interfaces, 2020. **12**(44): p. 50052-50060.

64. Vanaei, H., et al., *Influence of process parameters on thermal and mechanical properties of polylactic acid fabricated by fused filament fabrication.* Polymer Engineering & Science, 2020. **60**(8): p. 1822-1831.
65. Zanjanijam, A.R., et al., *Fused Filament Fabrication of PEEK: A Review of Process-Structure-Property Relationships.* Polymers, 2020. **12**(8): p. 1665.
66. Domingo-Espin, M., et al., *Fatigue Performance of ABS Specimens Obtained by Fused Filament Fabrication.* Materials, 2018. **11**(12): p. 2521.
67. Nienhaus, V., et al., *Investigations on nozzle geometry in fused filament fabrication.* Additive Manufacturing, 2019. **28**: p. 711-718.
68. Liu, X., et al., *Mechanical property parametric appraisal of fused deposition modeling parts based on the gray Taguchi method.* The International Journal of Advanced Manufacturing Technology, 2017. **89**(5): p. 2387-2397.
69. Slavkovic, V., et al. *Influence of annealing and printing directions on mechanical properties of PLA shape memory polymer produced by fused deposition modeling*. in *Proceedings of the 6th International Congress of Serbian Society of Mechanics Mountain Tara, Mountain Tara, Serbia*. 2017.
70. Galantucci, L.M., et al., *Analysis of dimensional performance for a 3D open-source printer based on fused deposition modeling technique.* Procedia Cirp, 2015. **28**: p. 82-87.
71. Bryll, K., et al. *Polymer composite manufacturing by FDM 3D printing technology*. in *MATEC Web of Conferences*. 2018. EDP Sciences.
72. Alharbi, N., R. Osman, and D. Wismeijer, *Effects of build direction on the mechanical properties of 3D-printed complete coverage interim dental restorations.* The Journal of Prosthetic Dentistry, 2016. **115**(6): p. 760-767.
73. Arnold, C., et al., *Surface Quality of 3D-Printed Models as a Function of Various Printing Parameters.* Materials, 2019. **12**(12): p. 1970.
74. Hada, T., et al., *Effect of printing direction on the accuracy of 3D-printed dentures using stereolithography technology.* Materials, 2020. **13**(15): p. 3405.
75. Cekic, A., et al., *OPTIMIZATION OF STEREOLITHOGRAPHY AND FUSED DEPOSITION MODELING PROCESS PARAMETERS.* Annals of DAAAM & Proceedings, 2019. **30**.
76. Zhao, T., et al., *4D printing of shape memory polyurethane via stereolithography.* European Polymer Journal, 2018. **101**: p. 120-126.
77. Seo, J.W., et al., *Hydrogel Production Platform with Dynamic Movement Using Photo-Crosslinkable/Temperature Reversible Chitosan Polymer and Stereolithography 4D Printing Technology.* Tissue Engineering and Regenerative Medicine, 2020. **17**(4): p. 423-431.
78. Zhao, J., M. Han, and L. Li, *Modeling and characterization of shape memory properties and decays for 4D printed parts using stereolithography.* Materials & Design, 2021. **203**: p. 109617.
79. Danish, M., et al., *4D printed stereolithography printed plant-based sustainable polymers: Preliminary investigation and optimization.* Journal of Applied Polymer Science, 2021. **138**(36): p. 50903.
80. Choong, Y.Y.C., et al., *Curing characteristics of shape memory polymers in 3D projection and laser stereolithography.* Virtual and Physical Prototyping, 2017. **12**(1): p. 77-84.
81. Shan, W., et al., *4D printing of shape memory polymer via liquid crystal display (LCD) stereolithographic 3D printing.* Materials Research Express, 2020. **7**(10): p. 105305.
82. Choong, Y.Y.C., et al., *4D printing of high performance shape memory polymer using stereolithography.* Materials & Design, 2017. **126**: p. 219-225.

83. Abdulhameed, O., et al., *Additive manufacturing: Challenges, trends, and applications.* Advances in Mechanical Engineering, 2019. **11**(2): p. 1687814018822880.
84. Peng, B., et al., *Digital Light Processing 3D Printing of Triple Shape Memory Polymer for Sequential Shape Shifting.* ACS Materials Letters, 2019. **1**(4): p. 410-417.
85. Fang, Z., et al., *Modular 4D Printing via Interfacial Welding of Digital Light-Controllable Dynamic Covalent Polymer Networks.* Matter, 2020. **2**(5): p. 1187-1197.
86. Zhang, B., et al., *Mechanically Robust and UV-Curable Shape-Memory Polymers for Digital Light Processing Based 4D Printing.* Advanced Materials, 2021. **33**(27): p. 2101298.
87. Mu, Q., et al., *Digital light processing 3D printing of conductive complex structures.* Additive Manufacturing, 2017. **18**: p. 74-83.
88. Ge, L., et al., *A digital light processing 3D printer for fast and high-precision fabrication of soft pneumatic actuators.* Sensors and Actuators A: Physical, 2018. **273**: p. 285-292.
89. Chen, Z., et al., *Recyclable thermosetting polymers for digital light processing 3D printing.* Materials & Design, 2021. **197**: p. 109189.
90. Cortés, A., et al., *DLP 4D-Printing of Remotely, Modularly, and Selectively Controllable Shape Memory Polymer Nanocomposites Embedding Carbon Nanotubes.* Advanced Functional Materials, 2021. **31**(50): p. 2106774.
91. Wu, H., et al., *Four-dimensional printing of a novel acrylate-based shape memory polymer using digital light processing.* Materials & Design, 2019. **171**: p. 107704.
92. Zhou, J. and S.S. Sheiko, *Reversible shape-shifting in polymeric materials.* Journal of Polymer Science Part B: Polymer Physics, 2016. **54**(14): p. 1365-1380.
93. *4D Printing Technology: A Review.* 3D Printing and Additive Manufacturing, 2015. **2**(4): p. 159-167.
94. Ehrmann, G. and A. Ehrmann, *3D printing of shape memory polymers.* Journal of Applied Polymer Science, 2021. **138**(34): p. 50847.
95. Panahi-Sarmad, M., et al., *Deep focusing on the role of microstructures in shape memory properties of polymer composites: A critical review.* European Polymer Journal, 2019. **117**: p. 280-303.
96. Xia, Y., et al., *A Review of Shape Memory Polymers and Composites: Mechanisms, Materials, and Applications.* Advanced Materials, 2021. **33**(6): p. 2000713.
97. Gopinath, S., et al., *One-way thermo-responsive shape memory polymer nanocomposite derived from polycaprolactone and polystyrene-block-polybutadiene-block-polystyrene packed with carbon nanofiber.* Materials Today Communications, 2020. **22**: p. 100802.
98. Hager, M.D., et al., *Shape memory polymers: Past, present and future developments.* Progress in Polymer Science, 2015. **49-50**: p. 3-33.
99. Fan, J. and G. Li, *High performance and tunable artificial muscle based on two-way shape memory polymer.* RSC advances, 2017. **7**(2): p. 1127-1136.
100. Zare, M., et al., *Thermally-induced two-way shape memory polymers: Mechanisms, structures, and applications.* Chemical Engineering Journal, 2019. **374**: p. 706-720.
101. Lee, A.Y., J. An, and C.K. Chua, *Two-Way 4D Printing: A Review on the Reversibility of 3D-Printed Shape Memory Materials.* Engineering, 2017. **3**(5): p. 663-674.
102. Rafiee, M., R.D. Farahani, and D. Therriault, *Multi-Material 3D and 4D Printing: A Survey.* Advanced Science, 2020. **7**(12): p. 1902307.
103. Lei, M., et al., *Recent progress in shape memory polymer composites: methods, properties, applications and prospects.* Nanotechnology Reviews, 2019. **8**(1): p. 327-351.

104. Chien, Y.-c., et al., *Preparation, Characterization, and Mechanism for Biodegradable and Biocompatible Polyurethane Shape Memory Elastomers.* ACS Applied Materials & Interfaces, 2017. **9**(6): p. 5419-5429.
105. Khalid, M.Y., et al., *4D printing of shape memory polymer composites: A review on fabrication techniques, applications, and future perspectives.* Journal of Manufacturing Processes, 2022. **81**: p. 759-797.
106. Lee, A.Y., et al., *Preliminary Investigation of the Reversible 4D Printing of a Dual-Layer Component.* Engineering, 2019. **5**(6): p. 1159-1170.
107. Wang, Y.-J., U.S. Jeng, and S.-h. Hsu, *Biodegradable Water-Based Polyurethane Shape Memory Elastomers for Bone Tissue Engineering.* ACS Biomaterials Science & Engineering, 2018. **4**(4): p. 1397-1406.
108. Li, M., et al., *Electroactive anti-oxidant polyurethane elastomers with shape memory property as non-adherent wound dressing to enhance wound healing.* Chemical Engineering Journal, 2019. **375**: p. 121999.
109. Raasch, J., et al., *Characterization of polyurethane shape memory polymer processed by material extrusion additive manufacturing.* Additive Manufacturing, 2015. **8**: p. 132-141.
110. Salimon, A.I., et al., *Chapter 6 - Shape memory polymer blends and composites for 3D and 4D printing applications*, in *3D and 4D Printing of Polymer Nanocomposite Materials*, K.K. Sadasivuni, K. Deshmukh, and M.A. Almaadeed, Editors. 2020, Elsevier. p. 161-189.
111. Karger-Kocsis, J. and S. Kéki, *Review of Progress in Shape Memory Epoxies and Their Composites.* Polymers, 2018. **10**(1): p. 34.
112. Song, J.J., H.H. Chang, and H.E. Naguib, *Design and characterization of biocompatible shape memory polymer (SMP) blend foams with a dynamic porous structure.* Polymer, 2015. **56**: p. 82-92.
113. Wallin, T., et al., *Click chemistry stereolithography for soft robots that self-heal.* Journal of Materials Chemistry B, 2017. **5**(31): p. 6249-6255.
114. Kim, H., et al., *3D printing of polyvinylidene fluoride/photopolymer resin blends for piezoelectric pressure sensing application using the stereolithography technique.* MRS Communications, 2019. **9**(3): p. 1115-1123.
115. Shaffer, S., et al., *On reducing anisotropy in 3D printed polymers via ionizing radiation.* Polymer, 2014. **55**(23): p. 5969-5979.
116. Wei, H., et al., *Direct-Write Fabrication of 4D Active Shape-Changing Structures Based on a Shape Memory Polymer and Its Nanocomposite.* ACS Applied Materials & Interfaces, 2017. **9**(1): p. 876-883.
117. Ge, Q., et al., *Multimaterial 4D Printing with Tailorable Shape Memory Polymers.* Scientific Reports, 2016. **6**(1): p. 31110.
118. Teoh, J.E.M., et al., *Hierarchically self-morphing structure through 4D printing.* Virtual and Physical Prototyping, 2017. **12**(1): p. 61-68.
119. Joanne Ee Mei, T., et al., *A preliminary investigation on cross-foldable design in 4D printing*, 2018.
120. Chen, S., Q. Zhang, and J. Feng, *3D printing of tunable shape memory polymer blends.* J. Mater. Chem. C, 2017. **5**.
121. Invernizzi, M., et al., *4D printed thermally activated self-healing and shape memory polycaprolactone-based polymers.* European Polymer Journal, 2018. **101**: p. 169-176.
122. Zhang, Y., et al., *3D printing of thermoreversible polyurethanes with targeted shape memory and precise in situ self-healing properties.* Journal of Materials Chemistry A, 2019. **7**(12): p. 6972-6984.
123. Ambulo, C.P., et al., *Four-dimensional Printing of Liquid Crystal Elastomers.* ACS Applied Materials & Interfaces, 2017. **9**(42): p. 37332-37339.

124. Kotikian, A., et al., *3D Printing of Liquid Crystal Elastomeric Actuators with Spatially Programed Nematic Order.* Advanced Materials, 2018. **30**(10): p. 1706164.
125. Wang, Z., et al., *Three-dimensional printing of functionally graded liquid crystal elastomer.* Science Advances, 2020. **6**(39): p. eabc0034.
126. Miao, S., et al., *4D printing smart biomedical scaffolds with novel soybean oil epoxidized acrylate.* Scientific Reports, 2016. **6**(1): p. 27226.
127. Cvetkovic, C., et al., *Three-dimensionally printed biological machines powered by skeletal muscle.* Proceedings of the National Academy of Sciences, 2014. **111**(28): p. 10125-10130.
128. Dong, S.-L., et al., *3D Printing of Aniline Tetramer-Grafted-Polyethylenimine and Pluronic F127 Composites for Electroactive Scaffolds.* Macromolecular Rapid Communications, 2017. **38**(4): p. 1600551.
129. Wang, Y., et al., *Three-dimensional printing of shape memory hydrogels with internal structure for drug delivery.* Materials Science and Engineering: C, 2018. **84**: p. 44-51.
130. Raviv, D., et al., *Active printed materials for complex self-evolving deformations.* Scientific reports, 2014. **4**(1): p. 1-8.
131. Chen, C., et al., *Collagen/heparin sulfate scaffolds fabricated by a 3D bioprinter improved mechanical properties and neurological function after spinal cord injury in rats.* Journal of Biomedical Materials Research Part A, 2017. **105**(5): p. 1324-1332.
132. Placone, J.K., et al., *Development and Characterization of a 3D Printed, Keratin-Based Hydrogel.* Annals of Biomedical Engineering, 2017. **45**(1): p. 237-248.
133. Hashmi, S., *Comprehensive materials processing*. 2014: Newnes.
134. Kianian, B. *Wohlers Report 2017: 3D Printing and Additive Manufacturing State of the Industry, Annual Worldwide Progress Report: Chapters titles: The Middle East, and other countries*. 2017.
135. Fitzharris, E.R., et al., *Effects of material properties on warpage in fused deposition modeling parts.* The International Journal of Advanced Manufacturing Technology, 2018. **95**(5): p. 2059-2070.
136. Bellehumeur, C., et al., *Modeling of Bond Formation Between Polymer Filaments in the Fused Deposition Modeling Process.* Journal of Manufacturing Processes, 2004. **6**(2): p. 170-178.
137. Hwang, S., et al., *Thermo-mechanical Characterization of Metal/Polymer Composite Filaments and Printing Parameter Study for Fused Deposition Modeling in the 3D Printing Process.* Journal of Electronic Materials, 2015. **44**(3): p. 771-777.
138. Kaiser, W., *Kunststoffchemie für Ingenieure: Von der Synthese bis zur Anwendung*. 2015: Hanser.
139. Bose, S., et al., *Additive manufacturing of biomaterials.* Progress in Materials Science, 2018. **93**: p. 45-111.
140. Plott, J. and A. Shih, *The extrusion-based additive manufacturing of moisture-cured silicone elastomer with minimal void for pneumatic actuators.* Additive Manufacturing, 2017. **17**: p. 1-14.
141. Zander, N.E., M. Gillan, and R.H. Lambeth, *Recycled polyethylene terephthalate as a new FFF feedstock material.* Additive Manufacturing, 2018. **21**: p. 174-182.
142. Stoof, D. and K.L. Pickering, *3D Printing of Natural Fibre Reinforced Recycled Polypropylene*, in *Processing and Fabrication of Advanced Materials - XXV*, S. Bickerton, et al., Editors. 2017, The University of Auckland: University of Auckland, Auckland, New Zealand. p. 668-691.
143. Cano, S., et al., *Additive manufacturing of zirconia parts by fused filament fabrication and solvent debinding: Selection of binder formulation.* Additive Manufacturing, 2019. **26**: p. 117-128.

144. Gonzalez-Gutierrez, J., et al., *Additive Manufacturing of Metallic and Ceramic Components by the Material Extrusion of Highly-Filled Polymers: A Review and Future Perspectives.* Materials, 2018. **11**(5): p. 840.
145. Hämäläinen, J.P., *Semi-crystalline polyolefins in fused deposition modeling*, 2017.
146. Antoine, L.D., C. Guillaume, and C. Mickaël, *Impression 3D/4D de matériaux composites thermoplastiques.* 2021(ref. article : bm7922).
147. Ning, F., et al., *Additive manufacturing of carbon fiber reinforced thermoplastic composites using fused deposition modeling.* Composites Part B: Engineering, 2015. **80**: p. 369-378.
148. Tekinalp, H.L., et al., *Highly oriented carbon fiber–polymer composites via additive manufacturing.* Composites Science and Technology, 2014. **105**: p. 144-150.
149. Tian, X., et al., *Interface and performance of 3D printed continuous carbon fiber reinforced PLA composites.* Composites Part A: Applied Science and Manufacturing, 2016. **88**: p. 198-205.
150. Gu, J., et al., *Thermo-mechanical modeling of woven fabric reinforced shape memory polymer composites.* Mechanics of Advanced Materials and Structures, 2019. **26**(12): p. 1042-1052.
151. Blok, L.G., et al., *An investigation into 3D printing of fibre reinforced thermoplastic composites.* Additive Manufacturing, 2018. **22**: p. 176-186.
152. Dong, K., et al., *Mechanical properties and shape memory effect of 4D printed cellular structure composite with a novel continuous fiber-reinforced printing path.* Materials & Design, 2021. **198**: p. 109303.
153. Leng, J., et al., *Shape-memory polymers and their composites: Stimulus methods and applications.* Progress in Materials Science, 2011. **56**(7): p. 1077-1135.
154. Zeng, C., et al., *4D printed electro-induced continuous carbon fiber reinforced shape memory polymer composites with excellent bending resistance.* Composites Part B: Engineering, 2020. **194**: p. 108034.
155. Lin, C., et al., *4D printing of shape memory polybutylene succinate/polylactic acid (PBS/PLA) and its potential applications.* Composite Structures, 2022. **279**: p. 114729.
156. Éditions, T.D.E.L.I., *Impression 3D de matériaux composites à matrice polymère Revue et prospective.* 2020(ref. article : bm7923).
157. Carneiro, O.S., A.F. Silva, and R. Gomes, *Fused deposition modeling with polypropylene.* Materials & Design, 2015. **83**: p. 768-776.
158. Love, L.J., et al., *The importance of carbon fiber to polymer additive manufacturing.* Journal of Materials Research, 2014. **29**(17): p. 1893-1898.
159. Guo, J., et al., *Shape memory and thermo-mechanical properties of shape memory polymer/carbon fiber composites.* Composites Part A: Applied Science and Manufacturing, 2015. **76**: p. 162-171.
160. Sun, J., Y. Liu, and J. Leng, *Mechanical properties of shape memory polymer composites enhanced by elastic fibers and their application in variable stiffness morphing skins.* Journal of Intelligent Material Systems and Structures, 2015. **26**(15): p. 2020-2027.
161. Rahman, A.A., T. Ikeda, and A. Senba, *Memory effects performance of polyurethane shape memory polymer composites (SMPC) in the variation of fiber volume fractions.* Fibers and Polymers, 2017. **18**(5): p. 979-986.
162. Lan, X., et al., *Fiber reinforced shape-memory polymer composite and its application in a deployable hinge.* Smart Materials and Structures, 2009. **18**(2): p. 024002.
163. Jordan, J., et al., *Experimental trends in polymer nanocomposites—a review.* Materials Science and Engineering: A, 2005. **393**(1): p. 1-11.

164. Liu, Y., et al., *Thermomechanics of shape memory polymer nanocomposites.* Mechanics of Materials, 2004. **36**(10): p. 929-940.
165. Ni, Q.-Q., et al., *Shape memory effect and mechanical properties of carbon nanotube/shape memory polymer nanocomposites.* Composite Structures, 2007. **81**(2): p. 176-184.
166. Wu, A.S., et al., *3D Printed Silicones with Shape Memory.* Scientific Reports, 2017. **7**(1): p. 4664.
167. Chen, K., et al., *Fabrication of tough epoxy with shape memory effects by UV-assisted direct-ink write printing.* Soft Matter, 2018. **14**(10): p. 1879-1886.
168. Sun, J., et al., *Synthesis and characterization of biocompatible Fe3O4 nanoparticles.* Journal of biomedical materials research Part A, 2007. **80**(2): p. 333-341.
169. Wang, Y.J., U.S. Jeng, and S.H. Hsu, *Biodegradable Water-Based Polyurethane Shape Memory Elastomers for Bone Tissue Engineering.* ACS Biomater Sci Eng, 2018. **4**(4): p. 1397-1406.
170. Yuan, C., et al., *3D printing of multi-material composites with tunable shape memory behavior.* Materials & Design, 2020. **193**: p. 108785.
171. Kashyap, D., P. Kishore Kumar, and S. Kanagaraj, *4D printed porous radiopaque shape memory polyurethane for endovascular embolization.* Additive Manufacturing, 2018. **24**: p. 687-695.
172. Su, J.-W., et al., *4D printing of polyurethane paint-based composites.* International Journal of Smart and Nano Materials, 2019. **10**(3): p. 237-248.
173. Wang, Y. and X. Li, *4D-printed bi-material composite laminate for manufacturing reversible shape-change structures.* Composites Part B: Engineering, 2021. **219**: p. 108918.
174. Kabir, S. and S. Lee, *Study of Shape Memory and Tensile Property of 3D Printed Sinusoidal Sample/Nylon Composite Focused on Various Thicknesses and Shape Memory Cycles.* Polymers, 2020. **12**(7): p. 1600.
175. Rodriguez, J.N., et al., *Shape-morphing composites with designed micro-architectures.* Scientific Reports, 2016. **6**(1): p. 27933.
176. Wei, H., et al., *Direct 3D printing of hybrid nanofiber-based nanocomposites for highly conductive and shape memory applications.* ACS applied materials & interfaces, 2019. **11**(27): p. 24523-24532.
177. Wan, X., et al., *CNT-based electro-responsive shape memory functionalized 3D printed nanocomposites for liquid sensors.* Carbon, 2019. **155**: p. 77-87.
178. Garcia Rosales, C.A., et al., *3D printing of shape memory polymer (SMP)/carbon black (CB) nanocomposites with electro-responsive toughness enhancement.* Materials Research Express, 2018. **5**(6): p. 065704.
179. Zhao, W., et al., *Personalized 4D printing of bioinspired tracheal scaffold concept based on magnetic stimulated shape memory composites.* Composites Science and Technology, 2019. **184**: p. 107866.
180. Zhang, Y., et al., *4D Printing of Magnetoactive Soft Materials for On-Demand Magnetic Actuation Transformation.* ACS Applied Materials & Interfaces, 2021. **13**(3): p. 4174-4184.
181. Wu, H., et al., *Selective Laser Sintering-Based 4D Printing of Magnetism-Responsive Grippers.* ACS Applied Materials & Interfaces, 2020. **13**(11): p. 12679-12688.
182. Wang, J., et al., *Facile fabrication of near-infrared light-responsive shape memory nanocomposite scaffolds with hierarchical porous structures.* Journal of Applied Polymer Science, 2021. **138**(37): p. 50938.
183. Leng, J., X. Wu, and Y. Liu, *Infrared light‐active shape memory polymer filled with nanocarbon particles.* Journal of Applied Polymer Science, 2009. **114**(4): p. 2455-2460.

184. Ponyrko, S., R. Donato, and L. Matějka, *Tailored high performance shape memory epoxy–silica nanocomposites. Structure design.* Polymer Chemistry, 2016. **7**(3): p. 560-572.
185. Lee, S.K., et al., *Waterborne polyurethane nanocomposites having shape memory effects.* Journal of Polymer Science Part A: Polymer Chemistry, 2011. **49**(3): p. 634-641.
186. Auad, M.L., et al., *Characterization of nanocellulose‐reinforced shape memory polyurethanes.* Polymer International, 2008. **57**(4): p. 651-659.
187. Xu, B., et al., *Thermal-mechanical properties of polyurethane-clay shape memory polymer nanocomposites.* Polymers, 2010. **2**(2): p. 31-39.
188. Hassanzadeh-Aghdam, M.K. and R. Ansari, *Thermal conductivity of shape memory polymer nanocomposites containing carbon nanotubes: A micromechanical approach.* Composites Part B: Engineering, 2019. **162**: p. 167-177.
189. Ang, J.Y., et al., *Engineering Porous Water-Responsive Poly(PEG/PCL/PDMS Urethane) Shape Memory Polymers.* Macromolecular Materials and Engineering, 2017. **302**(9): p. 1700174.
190. Lee, M.E. and A.M. Armani, *Flexible UV Exposure Sensor Based on UV Responsive Polymer.* ACS Sensors, 2016. **1**(10): p. 1251-1255.
191. Xie, Y., et al., *Bistable and Reconfigurable Photonic Crystals—Electroactive Shape Memory Polymer Nanocomposite for Ink-Free Rewritable Paper.* Advanced Functional Materials, 2018. **28**(34): p. 1802430.
192. Zolfagharian, A., et al., *3D/4D-printed bending-type soft pneumatic actuators: fabrication, modelling, and control.* Virtual and Physical Prototyping, 2020. **15**(4): p. 373-402.
193. Duan, A., et al., *3D-printable thermochromic acrylic resin with excellent mechanical performance.* Journal of Applied Polymer Science, 2020. **137**(2): p. 48277.
194. Han, D., et al., *Micro 3D Printing of a Temperature-Responsive Hydrogel Using Projection Micro-Stereolithography.* Scientific Reports, 2018. **8**(1): p. 1963.
195. Mao, Y., et al., *Sequential Self-Folding Structures by 3D Printed Digital Shape Memory Polymers.* Scientific Reports, 2015. **5**(1): p. 13616.
196. Senatov, F.S., et al., *Mechanical properties and shape memory effect of 3D-printed PLA-based porous scaffolds.* Journal of the Mechanical Behavior of Biomedical Materials, 2016. **57**: p. 139-148.
197. Dong, K., et al., *Electro-induced shape memory effect of 4D printed auxetic composite using PLA/TPU/CNT filament embedded synergistically with continuous carbon fiber: A theoretical & experimental analysis.* Composites Part B: Engineering, 2021. **220**: p. 108994.
198. Huang, X., et al., *Tracing evolutions in electro-activated shape memory polymer composites with 4D printing strategies: A systematic review.* Composites Part A: Applied Science and Manufacturing, 2021. **147**: p. 106444.
199. Garces, I.T. and C. Ayranci, *A view into additive manufactured electro-active reinforced smart composite structures.* Manufacturing Letters, 2018. **16**: p. 1-5.
200. Lu, X., et al., *4D-Printing of Photoswitchable Actuators.* Angewandte Chemie International Edition, 2021. **60**(10): p. 5536-5543.
201. Zolfagharian, A., et al., *Topology-Optimized 4D Printing of a Soft Actuator.* Acta Mechanica Solida Sinica, 2020. **33**(3): p. 418-430.
202. Chen, D., et al., *4D Printing Strain Self-Sensing and Temperature Self-Sensing Integrated Sensor–Actuator with Bioinspired Gradient Gaps.* Advanced Science, 2020. **7**(13): p. 2000584.
203. Tang, Y., et al., *Recent Advances of 4D Printing Technologies Toward Soft Tactile Sensors.* Frontiers in Materials, 2021. **8**: p. 110.

204. Bar-Cohen, Y., *Electroactive polymer (EAP) actuators as artificial muscles: reality, potential, and challenges*. Vol. 136. 2004: SPIE press.
205. Lendlein, A. and O.E.C. Gould, *Reprogrammable recovery and actuation behaviour of shape-memory polymers.* Nature Reviews Materials, 2019. **4**(2): p. 116-133.
206. Duduta, M., et al., *Realizing the potential of dielectric elastomer artificial muscles.* Proceedings of the National Academy of Sciences, 2019. **116**(7): p. 2476-2481.
207. Du, F.-P., et al., *Electroactive shape memory polymer based on optimized multi-walled carbon nanotubes/polyvinyl alcohol nanocomposites.* Composites Part B: Engineering, 2015. **68**: p. 170-175.
208. Chang, L., et al., *Ionic electroactive polymers used in bionic robots: a review.* Journal of Bionic Engineering, 2018. **15**(5): p. 765-782.
209. Wang, Z., et al., *3D Printing of Electrically Responsive PVC Gel Actuators.* ACS Applied Materials & Interfaces, 2021. **13**(20): p. 24164-24172.
210. Ze, Q., et al., *Shape Memory Polymers: Magnetic Shape Memory Polymers with Integrated Multifunctional Shape Manipulation (Adv. Mater. 4/2020).* Advanced Materials, 2020. **32**(4): p. 2070025.
211. Testa, P., et al., *Magnetically Addressable Shape-Memory and Stiffening in a Composite Elastomer.* Advanced Materials, 2019. **31**(29): p. 1900561.
212. Lantean, S., et al., *3D Printing of Magnetoresponsive Polymeric Materials with Tunable Mechanical and Magnetic Properties by Digital Light Processing.* Advanced Materials Technologies, 2019. **4**(11): p. 1900505.
213. Wu, H., et al., *Selective Laser Sintering-Based 4D Printing of Magnetism-Responsive Grippers.* ACS Applied Materials & Interfaces, 2021. **13**(11): p. 12679-12688.
214. Kim, T., et al., *Organic Photomechanical Materials.* Chemphyschem : a European journal of chemical physics and physical chemistry, 2014. **15**.
215. Nakano, H., R. Ichikawa, and R. Matsui, *Photomechanical Bending of Azobenzene-Based Photochromic Molecular Fibers.* Micromachines, 2013. **4**(2): p. 128-137.
216. Bai, Y., et al., *A reconfigurable, self-healing and near infrared light responsive thermoset shape memory polymer.* Composites Science and Technology, 2020. **187**: p. 107940.
217. Hu, Y., et al., *Botanical-Inspired 4D Printing of Hydrogel at the Microscale.* Advanced Functional Materials, 2020. **30**(4): p. 1907377.
218. Dutta, S. and D. Cohn, *Temperature and pH responsive 3D printed scaffolds.* Journal of Materials Chemistry B, 2017. **5**(48): p. 9514-9521.
219. Mirani, B., et al., *An Advanced Multifunctional Hydrogel-Based Dressing for Wound Monitoring and Drug Delivery.* Advanced Healthcare Materials, 2017. **6**(19): p. 1700718.
220. Nadgorny, M., et al., *Three-Dimensional Printing of pH-Responsive and Functional Polymers on an Affordable Desktop Printer.* ACS Applied Materials & Interfaces, 2016. **8**(42): p. 28946-28954.
221. Falahati, M., et al., *Smart polymers and nanocomposites for 3D and 4D printing.* Materials Today, 2020. **40**: p. 215-245.
222. Zhang, K., et al., *Moisture-responsive films of cellulose stearoyl esters showing reversible shape transitions.* Scientific Reports, 2015. **5**(1): p. 11011.
223. Baker, A.B., et al., *4D printing with robust thermoplastic polyurethane hydrogel-elastomer trilayers.* Materials & Design, 2019. **163**: p. 107544.
224. Kim, K., et al., *4D Printing of Hygroscopic Liquid Crystal Elastomer Actuators.* Small, 2021. **17**(23): p. 2100910.
225. Siqueira, G., et al., *Cellulose Nanocrystal Inks for 3D Printing of Textured Cellular Architectures.* Advanced Functional Materials, 2017. **27**(12): p. 1604619.

226. Correa, D., et al., *3D-printed wood: programming hygroscopic material transformations.* 3D Printing and Additive Manufacturing, 2015. **2**(3): p. 106-116.
227. Arif, Z.U., et al., *4D bioprinting of smart polymers for biomedical applications: recent progress, challenges, and future perspectives.* Reactive and Functional Polymers, 2022. **179**: p. 105374.
228. Haleem, A., et al., *Significant roles of 4D printing using smart materials in the field of manufacturing.* Advanced Industrial and Engineering Polymer Research, 2021.
229. Ahmed, A.A., A. Musbah, and A. Atiyah, *4D Printing Technology: A Revolution Across Manufacturing.* International Journal of Mechanical and Industrial Technology, 2020. **7**: p. 45-51.
230. Sydney Gladman, A., et al., *Biomimetic 4D printing.* Nature Materials, 2016. **15**(4): p. 413-418.
231. Chen, T. and K. Shea, *An autonomous programmable actuator and shape reconfigurable structures using bistability and shape memory polymers.* 3D Printing and Additive Manufacturing, 2018. **5**(2): p. 91-101.
232. Wang, J., et al., *Biomimetic Shape–Color Double-Responsive 4D Printing.* Advanced Materials Technologies, 2019. **4**(9): p. 1900293.
233. Miao, S., et al., *4D printing of polymeric materials for tissue and organ regeneration.* Materials Today, 2017. **20**(10): p. 577-591.
234. Apsite, I., et al., *4D Biofabrication of fibrous artificial nerve graft for neuron regeneration.* Biofabrication, 2020. **12**(3): p. 035027.
235. Rastogi, P. and B. Kandasubramanian, *Breakthrough in the printing tactics for stimuli-responsive materials: 4D printing.* Chemical Engineering Journal, 2019. **366**: p. 264-304.
236. Wang, Y., et al., *4D Printed Cardiac Construct with Aligned Myofibers and Adjustable Curvature for Myocardial Regeneration.* ACS Applied Materials & Interfaces, 2021. **13**(11): p. 12746-12758.
237. Schneider, L.A., et al., *Influence of pH on wound-healing: a new perspective for wound-therapy?* Archives of dermatological research, 2007. **298**(9): p. 413-420.
238. Walker, D.A., J.L. Hedrick, and C.A. Mirkin, *Rapid, large-volume, thermally controlled 3D printing using a mobile liquid interface.* Science, 2019. **366**(6463): p. 360-364.

Graphical abstract